Commit Locally, Exit Globally: Coordinating Adaptive Sampling and Early Exit in Diffusion Language Models

Chia-Ming Lee[1,2], **Shao-Kai Liu**[1], **Ming-Ching Chang**[2], **Xin Li**[2]
Yu-Lun Liu[1], **Chih-Chung Hsu**[1]
[1]National Yang Ming Chiao Tung University [2]University at Albany, SUNY

arXiv:2607.28166v2 [cs.CL] 13 Aug 2026

Abstract

Diffusion language models expose a provisional prediction at every denoising step, and on many tasks the candidate answer inside it stabilizes before the step schedule is exhausted. This creates two acceleration opportunities, leaving a block early and stopping the sequence early, but the two require different criteria because block acceleration is local whereas sequence termination is global and freezes the graded answer. Existing methods usually optimize only one axis, and existing exit gates rely on fixed-region confidence or schedule-dependent rules rather than the candidate answer itself. We present C^4, which coordinates the two axes by giving each decision its own gate. **Confidence-Verified Early Exit** (CVEE) decides *when* the sequence may stop, requiring confidence and sustained argmax stability over a candidate span re-extracted at every step. **Commit-Core-Then-Confirm** (CCTC) decides *which token positions* a step may commit by borrowing an autoregressive freezing order inside each block: it commits a boundary-anchored core and confirms deferred positions one step later, so the answer block can be accelerated without allowing local commits inside the answer span to determine sequence-level termination. On 12 zero-shot tasks with LLaDA and Dream, one frozen configuration removes 64–95% of decoding steps and delivers measured end-to-end speedups of 2.6× to 18.6× over full decoding. Code is available at https://github.com/ming053l/C4-dLLM.

1 Introduction

Diffusion language models (DLMs) generate text by iteratively denoising a fully-masked sequence rather than by extending a prefix left to right (Nie et al., 2025; Ye et al., 2025); accordingly, each step predicts masked token positions in parallel with bidirectional context. This decoding scheme exposes two sources of training-free slack. First, every denoising step already yields a *provisional* prediction for the whole sequence, and on many tasks the candidate answer inside it reaches its full-decoding value well before the last step. Second, practical DLM decoders run the generation region block by block under a semi-autoregressive schedule, with contiguous blocks decoded left to right; accordingly, the budget can be cut at two different scopes: a block may advance before its steps are exhausted, and the sequence may terminate before all blocks finish.

Leaving a block early and stopping the sequence early are not the same decision. The former is **local and bounded**, since later blocks can still write around whatever it fixed; the latter is **global and final**, filling every remaining token position, the graded answer included, in one step. The signal should therefore match the scope of the action it licenses: accelerating a block asks whether a token position has settled, whereas stopping asks whether the *answer* has. Existing accelerators usually optimize one control point and leave the other at its default schedule. *Adaptive-sampling* rules such as *Fast-dLLM* (Wu et al., 2026), *SlowFast Sampling* (Wei et al., 2026) and *KLASS* (Kim et al., 2025) accelerate commitment while decoding continues; generation-time *early-exit* rules such as *Prophet* (Li et al., 2026) and *SchED* (Mohamed et al., 2026b) decide when the sequence may stop, yet they decide from fixed-region confidence statistics or schedule-dependent rules rather than from the candidate answer

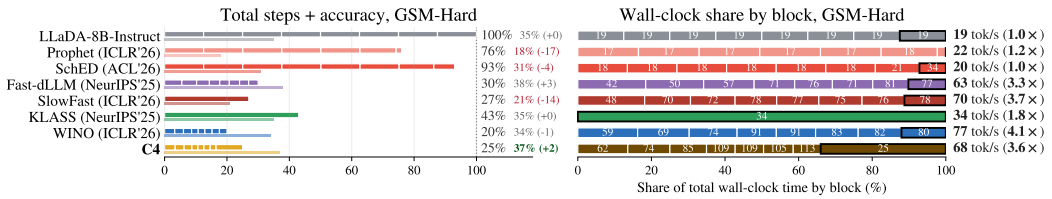

Figure 1: Bounded-accuracy acceleration. On GSM-Hard, C^4 reaches 37% accuracy (+2 points over full decoding) using 25% of the steps (left); the right panel decomposes estimated wall-clock share by block and reports measured aggregate TPS with paired-baseline speedup.

itself; and *WINO* (Hong et al., 2026) makes commits revocable by re-masking what a shadow block disputes, which reaches the sampling axis only.

This mismatch creates two distinct failure modes. First, neither the number of steps already taken nor an aggregate of token-level margins certifies that the answer has converged. Short-answer tasks meet an operational convergence criterion after roughly 4% of decoding, whereas multi-step tasks do not until the final 4%; prior exit gates therefore break down on long-reasoning settings because they stop on schedule- or margin-level proxies that can look settled before the answer itself has. Second, the two control points interact. The block carrying the graded answer is also a block a sampler would want to accelerate. Once an aggressive local rule commits inside that span, the answer is frozen by the sampler rather than settled by the model. **Local commitment inside the answer block can therefore contaminate the signal an early-exit gate tests**.

We therefore coordinate the two axes by giving each decision its own gate, thereby ensuring that local commitment never has to stand in for global termination. *Confidence-Verified Early Exit (CVEE)* decides *when* the sequence may stop by verifying answer-level convergence rather than relying on schedule- or margin-level proxies. At every step it re-extracts and relocates the candidate answer, permitting termination only when confidence and sustained argmax stability hold together over that span, thereby preventing a transiently stable guess from passing as the basis for sequence-wide termination.

Commit-Core-Then-Confirm (CCTC) decides *which token positions* a step may commit, and it is designed so that accelerating the answer block does not corrupt what CVEE verifies. Borrowing an autoregressive freezing order inside each block while keeping computation diffusion-style and parallel, it commits only a boundary-anchored core that tolerates a bounded number of still-masked token positions and rechecks deferred positions on the next step without an additional model evaluation. A token position inside the answer span is therefore committed only as part of a surviving run, never by one confident token alone. Separating the two decisions this way lets the methods compound: CCTC removes token-position slack without freezing the signal CVEE tests, and CVEE can terminate as soon as the accelerated answer span has genuinely settled.

- We show candidate stabilization is strongly task-dependent, early on short-answer tasks and only near the horizon on long-reasoning ones. A gate keyed to how far decoding has run or to fixed-region confidence therefore commits before the answer has stabilized, as Section 4.1 shows.
- We propose C^4, which commits locally and exits globally by treating the two as **separate decisions** with a gate apiece. *CVEE* verifies the extracted candidate before global termination, and *CCTC* commits a boundary-anchored core and confirms deferred positions one step later, thereby accelerating the answer span without freezing what CVEE verifies, in Sections 4.2 and 4.3.
- We evaluate it on 12 general short-answer, long-reasoning, and code-generation tasks on two model families under one frozen gate configuration, removing 64–95% of the steps and delivering measured end-to-end speedups of 2.6× to 18.6×, in Section 5.

2 Related Work

Diffusion language models. The diffusion framework traces to Sohl-Dickstein et al. (2015), extended to discrete data by Hoogeboom et al. (2021); Austin et al. (2021a); Campbell et al. (2022), with Lou et al. (2024) and the masked-diffusion line (Shi et al., 2024; Sahoo et al., 2024; Ou et al., 2025; Zheng et al., 2025) establishing the parameterizations LLaDA and Dream build on. LLaDA

(Nie et al., 2025) and Dream (Ye et al., 2025), the open-weight DLMs we evaluate on, expose a revisable prediction at every masked token position and admit an arbitrary step budget at inference; C^4 reduces that budget under block-wise decoding without prematurely terminating the candidate answer, by separating token-position commitment from answer-level termination.

Early exit and sequence termination. Early exit has been studied at the layer, reasoning-step, and token level. Gu et al. (2026) apply it to *depth* via hidden-state stabilization. Among autoregressive CoT methods, S-GRPO (Dai et al., 2025), DEER (Yang et al., 2026), CORE (Zhai et al., 2026), and BMC (Ruan et al., 2026) trigger early stopping via decaying reward, transition confidence, brittle-token revision, and geometric reconstruction, respectively. For DLMs, Prophet (Li et al., 2026) terminates generation once an aggregate confidence gap over a fixed monitoring region clears a staged threshold, and SchED (Mohamed et al., 2026b) smooths that trigger into a decay schedule; the decision that freezes the whole remaining sequence therefore does not explicitly track the candidate it freezes. C^4 instead conditions global termination on confidence and stability over a dynamically extracted candidate span.

Adaptive sampling for DLMs. This axis adjusts how many token positions commit per step while decoding continues. Fast-dLLM (Wu et al., 2026), SlowFast Sampling (Wei et al., 2026) and KLASS (Kim et al., 2025) each commit on a token-level statistic, and concurrent work refines the same signals: LESS (Mohamed et al., 2026a) pairs confidence with stability, STDec (Chen et al., 2026) adapts thresholds over spatial neighborhoods, TACG (Wang et al., 2026) uses EMA-logit trajectories, Swordsman (Zhang et al., 2026) re-partitions blocks along entropy shifts, R^2-dLLM (Du et al., 2026) finalizes stable tokens via spatio-temporal redundancy but requires fine-tuning, and Kim et al. (2026) trace commitment instability to a proximity bias in the denoising order. WINO (Hong et al., 2026) is the closest relative of the rule developed here, and the contrast is revocation against restraint. WINO writes wide and then re-masks disputed token positions, where our rule constrains the shape of a commit beforehand and never revokes. What none of these methods decide is whether the sequence is finished; consequently, a run they accelerate still decodes every remaining token.

3 Background and Problem Setup

DLM generation process. A DLM generates a sequence x_0 of length L by learning to reverse a discrete corruption process that progressively masks a clean sequence over forward time $u \in [0, 1]$,

$$q(x_u \mid x_0) = \prod_{i=1}^{L} q(x_u^i \mid x_0^i), \tag{1}$$

$$q(x_u^i \mid x_0^i) = \begin{cases} x_0^i, & \text{w.p. } 1-u, \quad \text{(a) token kept} \\ \texttt{[MASK]}, & \text{w.p. } u, \quad \text{(b) token masked} \end{cases} \tag{2}$$

so x_1 is fully masked and x_0 is the original sequence. The model $p_\theta(x_0 \mid x_u)$ learns to predict x_0 from any masked x_u; generation reverses this over T discrete *decoding steps* $t \in \{1, \ldots, T\}$, a separate index unrelated to forward time u. Each step produces a full prediction $\hat{x}$ for every masked position, then a *remasking* rule commits some subset permanently and leaves the rest masked. Since T is chosen at inference time, how many steps are used and what the remasking rule commits is the design space this paper targets.

Semi-autoregressive decoding. In practice, the masked process of Eqs. 1 and 2 is not run over the whole sequence at once. The generation region is partitioned into N equal contiguous blocks $B_0, \ldots, B_{N-1}$ and decoded left to right, each block denoised for $S = T/N$ steps before the next begins, so diffusion happens within a block and autoregression across blocks. This is the schedule used by both reference decoders, LLaDA-8B-Instruct (Nie et al., 2025) and Dream-7B-Instruct (Ye et al., 2025), and it creates the two control points we modify: when a block may be left and when the sequence may be stopped. Within a block, *low-confidence remasking* sets the schedule (t resets per block). Let $c_i^{(t)}$ be the model's softmax confidence in its top-1 prediction $\hat{x}_i^{(t)}$ at masked position i, and m the block's initial mask count; writing $q = \lfloor m/S \rfloor$ and $r = m \bmod S$, step t commits the $k_t = q + \mathbf{1}[t \le r]$ highest-confidence masked positions. The quota depends only on m and S, so the block is fully committed by step S whatever the model believes.

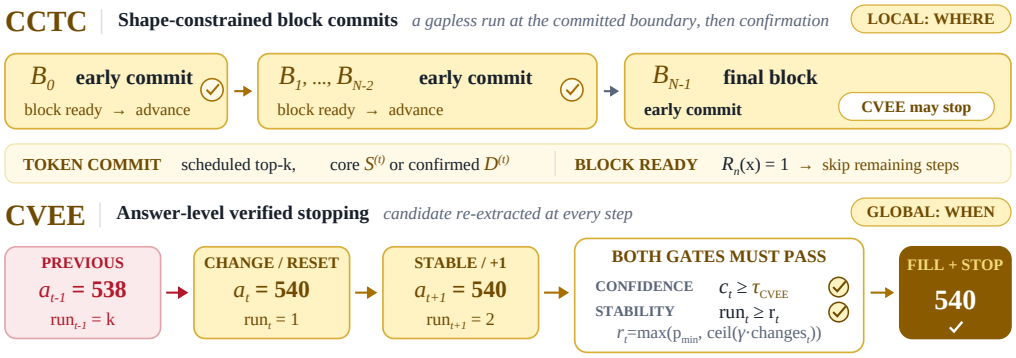

Figure 2: C^4 commits locally and exits globally. CCTC accelerates every block by committing a boundary-anchored core and confirming what it withheld one step later, including the final block so answer-block acceleration composes with CVEE rather than being withheld; CVEE independently decides whether the whole sequence may be filled and stopped. No block-local signal is allowed to certify answer-level convergence for the stop decision.

Early-termination gates. Prophet (Li et al., 2026) and SchED (Mohamed et al., 2026b) modify the second control point above, deciding when the whole sequence may stop and fill; the adaptive samplers of Section 2 instead adjust how quickly positions commit and never make that decision. Prophet averages the top-1/top-2 logit gap over a monitored region $\mathcal{R}$,

$$\bar{g}_t = \frac{1}{|\mathcal{R}|} \sum_{i \in \mathcal{R}} \left(\ell_i^{(t),1} - \ell_i^{(t),2} \right), \tag{3}$$

where $\ell_i^{(t),1}, \ell_i^{(t),2}$ are the two largest logits at position i and step t. Here, $\mathcal{R}$ is a task-format-specific monitoring region whose definition we hold fixed across our free-form evaluation and Prophet's suffix-prompt setting, as Appendix A.2 sets out. Prophet fills all remaining masked positions in a single step once $\bar{g}_t$ crosses its published three-stage threshold, which changes with decoding progress; SchED smooths this into a progress-dependent decay curve with a stability guard, still firing as one global fill. Both aggregate position-level signals into a single sequence-wide trigger.

4 Local Commitment and Global Exit

The design principle is to match the signal a gate uses to the scope of its decision. Token-level statistics can accelerate a block but cannot certify that a sequence should stop, whereas answer identity and stability can. *CVEE* therefore decides *when* to stop and *CCTC* *which token positions* a step may commit, and Figure 2 shows how the two savings combine.

4.1 Why Progress-Based Global Stopping Fails

Decoding progress is not the same as answer convergence. The cheapest exit gate stops at a fixed fraction of the step budget; accordingly, we first measure when a trajectory's answer actually stops moving. We take full LLaDA-8B-Instruct decodes drawn equally from MMLU, GSM8K and MATH. For each trajectory we ask when the extracted candidate *persistently* agrees with its own full-decoding output a_j^{full}. We write $s_j = \min\{s : a_{j,u} = a_j^{\text{full}} \; \forall u \geq s\}$ for trajectory j's *stabilization progress*, the progress after which the candidate never changes again, and s_p for the cohort progress by which a fraction p has reached its own s_j. The criterion is intentionally strict because the quantity of interest is when the candidate stops changing.

No single progress threshold works across tasks. Figure 3 shows $s_{0.9}$ running from 0.04 on short-answer tasks to 0.96 on long-reasoning ones. A fraction early enough for MMLU commits into an unfinished chain of thought; one late enough for MATH wastes most of the budget elsewhere. Tightening the criterion does not narrow the range; thus the spread is a property of the trajectories rather than of the threshold. A gate that stops at the right time therefore has to track the answer trajectory itself. That is why a rule built on the aggregate logit gap $\bar{g}_t$ in Eq. 3 can still fail here: the monitored region may look confident early even while the extracted candidate continues to change.

4.2 Confidence-Verified Early Exit: Deciding When to Stop

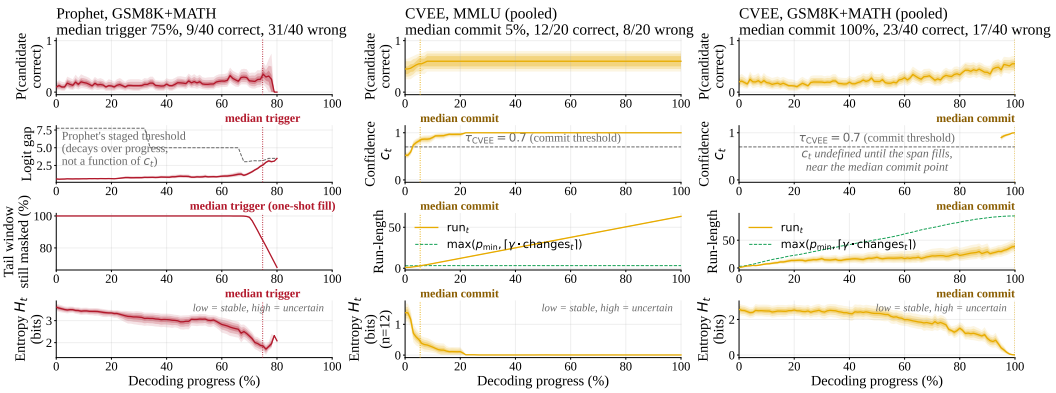

Figure 3: CVEE and Prophet gate trigger timing versus answer stabilization. Prophet's confidence gap rises well before the answer stops changing on GSM8K and MATH; accordingly, it fills while the model is still deciding. CVEE fires just as early on MMLU and waits on long-reasoning trajectories because its tested quantity has not settled. Predictive entropy at each trigger agrees: it is high where Prophet stops and near zero where CVEE does, so the disagreement concerns which quantity is tested rather than how strictly. Examples are excluded from CVEE's calibration.

Neither signal alone shows that an answer has converged. The gate must test the candidate itself. Here the *candidate* is what a deterministic parser returns at one step. Fixed by the task's output format, that parser locates the answer span inside the current prediction $\hat{x}^{(t)}$ and normalizes what it finds. The candidate therefore follows the answer as its span moves. The obvious criteria for testing it each fail on their own. A long unchanged run need not mean convergence, since LLaDA force-commits a fixed quota and a value can sit still by scheduling accident. High confidence has the opposite weakness: it carries no notion of time and cannot rule out a lucky guess. Early-exit methods outside DLM sampling run into the same problem. Methods for early exit in autoregressive reasoning likewise ask whether the reasoning is actually finished rather than trusting one instantaneous score to declare it so (Yang et al., 2026; Zhai et al., 2026; Ruan et al., 2026).

Confidence and candidate stability must hold jointly. CVEE lifts that pairing to the answer itself. At decoding step t let a_t be the extracted candidate; run_t the stability counter across successive same-value extractions (pausing rather than resetting when no candidate exists); changes_t the flip count; and $c_t \in [0, 1]$ the mean of the per-token confidences over the span that holds a_t. The gate fires at the first decoding step t satisfying

$$c_t \geq \tau_{\text{CVEE}} \qquad \text{(a) confidence gate}$$
$$\text{run}_t \geq \max\left(p_{\min}, \lceil \gamma \cdot \text{changes}_t \rceil\right) \qquad \text{(b) stability gate} \tag{4}$$

Termination requires both conditions to hold together: $p_{\min}$ blocks immediate commitment, and γ sets the extra stable steps each flip demands. All three hyperparameters ($\tau_{\text{CVEE}}, \gamma, p_{\min}$) are calibrated once on LLaDA and frozen, never retuned per task or model. None refers to the step budget or to how many steps have run; consequently, the gate is schedule-independent. The task dependence comes from the candidate trajectory itself: the gate stops after a few steps on short-answer tasks and waits near the horizon on long reasoning, because that is when those candidates settle. Nothing classifies the task first, unlike routers that allocate reasoning budgets per query (Lee et al., 2026).

4.3 Commit-Core-Then-Confirm: Where to Accelerate, and How Many to Commit

Threshold commits can leave the output incoherent. Let $E^{(t)}$ be the token positions whose confidence clears τ_{CCTC} at step t. If a token is unmasked while earlier positions still hold `[MASK]`, it is severed from unresolved left context and never re-decoded. Figure 4 shows why CCTC stays block-parallel under an autoregressive freezing order. Conceptually, threshold-ready positions are not always safe to freeze; accordingly, CCTC nevertheless keeps parallel prediction within the block, commits only from the boundary, defers later ready positions, and confirms them one step later.

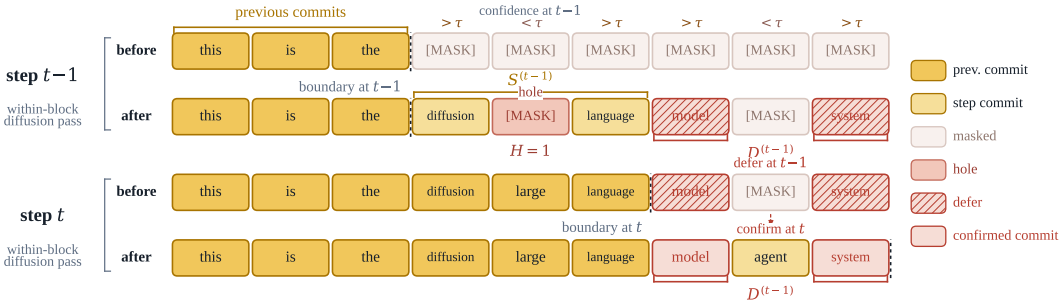

Figure 4: CCTC stays block-parallel under an autoregressive freezing order. At step t, the core $S^{(t)}$ commits from the committed boundary and may cross at most H holes; later ready positions stay masked and are deferred. At the same step, $D^{(t)}$ confirms positions deferred at $t-1$ only after the boundary has advanced into their left context.

Autoregressive freezing within a block. An autoregressive decoder never faces this failure; it freezes only content whose left context is already final. CCTC borrows that order inside each block while keeping masked-position prediction parallel. It therefore **commits only the core**, the boundary-anchored prefix of $E^{(t)}$ allowing at most H low-confidence holes:

$$h_i^{(t)} = \left|\{\, j \in B_n : j < i,\ x_j^{(t)} = \texttt{[MASK]},\ j \notin E^{(t)} \,\}\right|, \qquad S^{(t)} = \{\, i \in E^{(t)} : h_i^{(t)} \le H \,\}, \tag{5}$$

Here $h_i^{(t)}$ counts unresolved holes before i. Already-committed positions are not holes; accordingly, the core anchors at the boundary without extra bookkeeping. Positions beyond the H-th hole, $E^{(t)} \setminus S^{(t)}$, are **deferred**, held masked for one step with their predicted tokens recorded. Only the freezing order is autoregressive; masked-position prediction remains parallel.

Autoregressive safety at diffusion throughput. The **confirm** re-checks the deferred positions inside the next forward pass. $D^{(t+1)}$ collects the positions whose new prediction still matches the recorded token once the core sits in their left context; these commit at the next step. Unlike WINO (Hong et al., 2026), the rule never revokes and never adds a shadow verification pass. Write $\mathcal{A}$ for the blocks the rule accelerates and $\mathcal{K}^{(t)}$ for the scheduled top-k selection among the block's masked positions. Every masked $i \in B_n$ with $n \in \mathcal{A}$ then updates as

$$x_i^{(t+1)} = \begin{cases} \hat{x}_i^{(t)},\ i \in S^{(t)} \text{ (a) core} & \hat{x}_i^{(t)},\ i \in D^{(t)} \text{ (b) confirmed deferral} \\ \hat{x}_i^{(t)},\ i \in \mathcal{K}^{(t)} \text{ (c) scheduled top-}k & x_i^{(t)},\ \text{otherwise (d) stays masked} \end{cases} \tag{6}$$

Branch (c) guarantees progress; branches (a) and (b) add value-based commits as soon as the model resolves them. $H \to \infty$ makes $S^{(t)} = E^{(t)}$ and empties $D^{(t)}$; in that limit, the pure threshold rule returns exactly. Once every position in a block has committed the block is done. With $R_n(x) = \bigwedge_{i \in B_n} \left[x_i \neq \texttt{[MASK]}\right]$ checked against $x^{(t+1)}$, its remaining steps are skipped, a block-wise exit on the block's own signal.

Accelerating even the answer block. The last design choice is which blocks to accelerate. Withholding the final block, $\mathcal{A} = \{0, \ldots, N-2\}$, would avoid freezing inside the answer span. We instead deploy $\mathcal{A} = \{0, \ldots, N-1\}$, because positions there commit only as confirmed parts of a boundary-anchored run. CCTC can therefore accelerate the answer block without turning CVEE's stability test into a record of sampler decisions.

5 Experiments

Datasets and setup. We evaluate LLaDA-8B-Instruct (Nie et al., 2025) and Dream-7B-Instruct (Ye et al., 2025) with bf16, greedy decoding, and zero-shot prompting on a single RTX 4090. The 12 tasks span five *short-answer* benchmarks (MMLU (Hendrycks et al., 2021a), ARC-Challenge (Clark et al., 2018), HellaSwag (Zellers et al., 2019), WinoGrande (Sakaguchi et al., 2021), and PIQA (Bisk et al., 2020)), five *long-reasoning* benchmarks (GSM8K (Cobbe et al., 2021), MATH (Hendrycks et al., 2021b), SVAMP (Patel et al., 2021), ASDiv (Miao et al., 2020), and GSM-Hard (Gao et al., 2023)), and two *code-generation* benchmarks (HumanEval (Chen et al., 2021) and MBPP (Austin et al., 2021b), both graded by hidden unit-test pass/fail).

Task	Variant	LLaDA-8B-Instruct Acc (%)	Avg. Step	Saving	TPS	Speedup	Dream-7B-Instruct Acc (%)	Avg. Step	Saving	TPS	Speedup
General / short-answer tasks (single-token or short-span answers)											
MMLU	Baseline	64.0	64.0	0.0%	30.4	1.00×	71.5	64.0	0.0%	28.2	1.00×
(n=200, sequence length=64)	Prophet (Li et al., 2026)	62.5 (-1.5)	8.2 (-55.8)	87.2%	202.2	6.70×	71.5 (+0.0)	14.8 (-49.2)	76.9%	109.8	3.89×
(block=16, 4 blocks)	SchED (Mohamed et al., 2026b)	61.5 (-2.5)	31.0 (-33.0)	51.6%	53.3	1.76×	69.0 (-2.5)	12.9 (-51.1)	79.8%	178.7	6.33×
	SlowFast (Wei et al., 2026)	63.0 (-1.0)	17.9 (-46.1)	72.0%	130.4	4.28×	74.5 (+3.0)	9.6 (-54.4)	85.0%	196.9	6.97×
	KLASS (Kim et al., 2025)	62.5 (-1.5)	29.2 (-34.8)	54.4%	51.7	1.69×	72.5 (+1.0)	11.3 (-52.7)	82.3%	129.0	4.57×
	WINO (Hong et al., 2026)	61.0 (-3.0)	16.8 (-47.2)	73.8%	100.4	3.38×	–	–	–	–	–
	C^4	64.0 (+0.0)	4.8 (-59.2)	92.5%	490.4	16.16×	70.0 (-1.5)	4.5 (-59.5)	93.0%	389.7	13.82×
ARC-C	Baseline	86.5	64.0	0.0%	33.8	1.00×	87.5	64.0	0.0%	32.6	1.00×
(n=200, sequence length=64)	Prophet (Li et al., 2026)	86.0 (-0.5)	7.5 (-56.5)	88.3%	295.3	8.51×	86.0 (-1.5)	14.0 (-50.0)	78.1%	138.3	4.25×
(block=16, 4 blocks)	SchED (Mohamed et al., 2026b)	85.0 (-1.5)	41.1 (-22.9)	35.8%	57.5	1.65×	88.5 (+1.0)	11.0 (-53.0)	82.8%	215.1	6.61×
	SlowFast (Wei et al., 2026)	85.0 (-1.5)	23.7 (-40.3)	63.0%	107.3	3.08×	87.0 (-0.5)	10.4 (-53.6)	83.8%	219.4	6.75×
	KLASS (Kim et al., 2025)	87.0 (+0.5)	37.5 (-26.5)	41.4%	53.7	1.55×	88.5 (+1.0)	11.6 (-52.4)	81.9%	158.9	4.88×
	WINO (Hong et al., 2026)	84.0 (-2.5)	20.1 (-43.9)	68.6%	76.9	2.33×	–	–	–	–	–
	C^4	86.5 (+0.0)	3.9 (-60.1)	93.9%	483.3	14.28×	88.5 (+1.0)	4.2 (-59.8)	93.4%	565.7	17.37×
HellaSwag	Baseline	75.5	64.0	0.0%	20.8	1.00×	75.5	64.0	0.0%	22.1	1.00×
(n=200, sequence length=64)	Prophet (Li et al., 2026)	75.0 (-0.5)	6.0 (-58.0)	90.6%	223.4	10.74×	75.0 (-0.5)	16.2 (-47.8)	74.7%	82.0	3.72×
(block=16, 4 blocks)	SchED (Mohamed et al., 2026b)	75.5 (+0.0)	27.7 (-36.3)	56.7%	46.4	2.23×	75.0 (-0.5)	19.0 (-45.0)	70.3%	63.0	2.85×
	SlowFast (Wei et al., 2026)	77.0 (+1.5)	10.9 (-53.1)	83.0%	134.2	6.44×	72.5 (-3.0)	9.0 (-55.0)	85.9%	160.0	7.25×
	KLASS (Kim et al., 2025)	75.0 (-0.5)	19.4 (-44.6)	69.7%	56.5	2.72×	69.5 (-6.0)	11.3 (-52.7)	82.3%	94.0	4.25×
	WINO (Hong et al., 2026)	73.0 (-2.5)	12.9 (-51.1)	79.8%	79.0	3.83×	–	–	–	–	–
	C^4	75.5 (+0.0)	3.7 (-60.3)	94.2%	348.6	16.72×	75.5 (+0.0)	4.4 (-59.6)	93.1%	297.8	13.46×
WinoGrande	Baseline	75.5	64.0	0.0%	36.1	1.00×	71.5	64.0	0.0%	35.5	1.00×
(n=200, sequence length=64)	Prophet (Li et al., 2026)	76.0 (+0.5)	5.9 (-58.1)	90.8%	383.9	10.24×	69.5 (-2.0)	15.3 (-48.7)	76.1%	140.6	3.98×
(block=16, 4 blocks)	SchED (Mohamed et al., 2026b)	75.5 (+0.0)	5.8 (-58.2)	90.9%	447.1	11.77×	71.0 (-0.5)	2.1 (-61.9)	96.7%	1034.4	29.08×
	SlowFast (Wei et al., 2026)	77.5 (+2.0)	8.5 (-55.5)	86.7%	285.5	7.64×	71.0 (-0.5)	8.0 (-56.0)	87.5%	279.6	7.85×
	KLASS (Kim et al., 2025)	76.5 (+1.0)	13.3 (-50.7)	79.2%	160.0	4.21×	72.5 (+1.0)	7.6 (-56.4)	88.1%	236.8	6.68×
	WINO (Hong et al., 2026)	77.0 (+1.5)	10.1 (-53.9)	84.2%	176.1	5.00×	–	–	–	–	–
	C^4	75.5 (+0.0)	3.4 (-60.6)	94.7%	672.8	18.66×	71.5 (+0.0)	4.2 (-59.8)	93.4%	561.4	15.83×
PIQA	Baseline	81.5	64.0	0.0%	35.2	1.00×	87.5	64.0	0.0%	32.5	1.00×
(n=200, sequence length=64)	Prophet (Li et al., 2026)	82.0 (+0.5)	10.8 (-53.2)	83.1%	245.7	6.86×	87.5 (+0.0)	18.9 (-45.1)	70.5%	104.0	3.19×
(block=16, 4 blocks)	SchED (Mohamed et al., 2026b)	81.0 (-0.5)	24.5 (-39.5)	61.7%	98.6	2.81×	87.0 (-0.5)	17.1 (-46.9)	73.3%	129.1	3.97×
	SlowFast (Wei et al., 2026)	84.0 (+2.5)	10.0 (-54.0)	84.4%	205.2	5.95×	89.5 (+2.0)	9.1 (-54.9)	85.8%	209.2	6.42×
	KLASS (Kim et al., 2025)	81.5 (+0.0)	18.6 (-45.4)	70.9%	106.3	2.96×	91.5 (+4.0)	10.6 (-53.4)	83.4%	158.0	4.85×
	WINO (Hong et al., 2026)	81.0 (-0.5)	11.4 (-52.6)	82.2%	187.7	5.47×	–	–	–	–	–
	C^4	82.0 (+0.5)	3.6 (-60.4)	94.4%	546.5	15.52×	88.0 (+0.5)	3.5 (-60.5)	94.5%	575.7	17.69×
Long-reasoning tasks (multi-step CoT)											
GSM8K	Baseline	66.0	256.0	0.0%	19.0	1.00×	85.0	256.0	0.0%	21.2	1.00×
(n=100, sequence length=256)	Prophet (Li et al., 2026)	38.0 (-28.0)	185.0 (-71.0)	27.7%	22.6	1.19×	16.0 (-69.0)	76.1 (-179.9)	70.3%	67.0	3.16×
(block=32, 8 blocks)	SchED (Mohamed et al., 2026b)	59.0 (-7.0)	224.3 (-31.7)	12.4%	21.1	1.11×	18.0 (-67.0)	76.9 (-179.1)	70.0%	64.9	3.07×
	SlowFast (Wei et al., 2026)	41.0 (-25.0)	70.9 (-185.1)	72.3%	68.0	3.57×	20.0 (-65.0)	89.2 (-166.8)	65.2%	59.6	2.81×
	KLASS (Kim et al., 2025)	65.0 (-1.0)	105.5 (-150.5)	58.8%	34.5	1.82×	33.0 (-52.0)	96.5 (-159.5)	62.3%	37.2	1.75×
	WINO (Hong et al., 2026)	72.0 (+6.0)	49.2 (-206.8)	80.8%	76.6	4.07×	–	–	–	–	–
	C^4	64.0 (-2.0)	62.5 (-193.5)	75.6%	67.5	3.55×	85.0 (+0.0)	54.5 (-201.5)	78.7%	102.1	4.82×
MATH	Baseline	32.0	256.0	0.0%	17.8	1.00×	42.0	256.0	0.0%	19.4	1.00×
(n=100, sequence length=256)	Prophet (Li et al., 2026)	19.0 (-13.0)	192.7 (-63.3)	24.7%	21.4	1.20×	15.0 (-27.0)	164.9 (-91.1)	35.6%	26.7	1.38×
(block=32, 8 blocks)	SchED (Mohamed et al., 2026b)	26.0 (-6.0)	233.5 (-22.5)	8.8%	19.3	1.08×	33.0 (-9.0)	199.0 (-57.0)	22.3%	23.3	1.20×
	SlowFast (Wei et al., 2026)	24.0 (-8.0)	100.0 (-156.0)	60.9%	45.5	2.55×	9.0 (-33.0)	98.9 (-157.1)	61.4%	51.9	2.67×
	KLASS (Kim et al., 2025)	34.0 (+2.0)	133.9 (-122.1)	47.7%	26.1	1.46×	4.0 (-38.0)	98.7 (-157.3)	61.4%	40.3	2.08×
	WINO (Hong et al., 2026)	35.0 (+3.0)	81.7 (-174.3)	68.1%	42.8	2.42×	–	–	–	–	–
	C^4	33.0 (+1.0)	92.5 (-163.5)	63.9%	46.7	2.61×	42.0 (+0.0)	84.5 (-171.5)	67.0%	53.5	2.76×
SVAMP	Baseline	81.0	256.0	0.0%	19.3	1.00×	76.0	256.0	0.0%	21.4	1.00×
(n=100, sequence length=256)	Prophet (Li et al., 2026)	40.0 (-41.0)	160.1 (-95.9)	37.5%	27.5	1.42×	29.0 (-47.0)	48.8 (-207.2)	80.9%	76.1	3.57×
(block=32, 8 blocks)	SchED (Mohamed et al., 2026b)	70.0 (-11.0)	196.0 (-60.0)	23.4%	26.9	1.39×	20.0 (-56.0)	42.9 (-213.1)	83.2%	75.8	3.56×
	SlowFast (Wei et al., 2026)	46.0 (-35.0)	81.7 (-174.3)	68.1%	63.4	3.28×	67.0 (-9.0)	49.9 (-206.1)	80.5%	137.0	6.42×
	KLASS (Kim et al., 2025)	79.0 (-2.0)	96.4 (-159.6)	62.3%	39.9	2.07×	71.0 (-5.0)	58.1 (-197.9)	77.3%	71.0	3.33×
	WINO (Hong et al., 2026)	85.0 (+4.0)	45.6 (-210.4)	82.2%	81.0	4.24×	–	–	–	–	–
	C^4	81.0 (+0.0)	58.8 (-197.2)	77.0%	82.8	4.28×	75.0 (-1.0)	42.8 (-213.2)	83.3%	113.0	5.29×
ASDiv	Baseline	68.0	256.0	0.0%	19.4	1.00×	78.0	256.0	0.0%	21.4	1.00×
(n=100, sequence length=256)	Prophet (Li et al., 2026)	37.0 (-31.0)	163.7 (-92.3)	36.1%	29.5	1.52×	25.0 (-53.0)	54.8 (-201.2)	78.6%	122.5	5.75×
(block=32, 8 blocks)	SchED (Mohamed et al., 2026b)	60.0 (-8.0)	197.0 (-59.0)	23.0%	28.6	1.48×	17.0 (-61.0)	53.3 (-202.7)	79.2%	101.1	4.74×
	SlowFast (Wei et al., 2026)	34.0 (-34.0)	82.4 (-173.6)	67.8%	64.9	3.35×	52.0 (-26.0)	57.9 (-198.1)	77.4%	144.0	6.78×
	KLASS (Kim et al., 2025)	66.0 (-2.0)	100.8 (-155.2)	60.6%	40.7	2.10×	58.0 (-20.0)	67.2 (-188.8)	73.8%	65.4	3.07×
	WINO (Hong et al., 2026)	60.0 (-8.0)	48.2 (-207.8)	81.2%	84.5	4.41×	–	–	–	–	–
	C^4	71.0 (+3.0)	60.9 (-195.1)	76.2%	86.9	4.48×	76.0 (-2.0)	45.8 (-210.2)	82.1%	135.1	6.32×
GSM-Hard	Baseline	35.0	256.0	0.0%	18.8	1.00×	42.0	256.0	0.0%	20.6	1.00×
(n=100, sequence length=256)	Prophet (Li et al., 2026)	18.0 (-17.0)	194.1 (-61.9)	24.2%	21.9	1.16×	9.0 (-33.0)	103.9 (-152.1)	59.4%	45.7	2.22×
(block=32, 8 blocks)	SchED (Mohamed et al., 2026b)	31.0 (-4.0)	237.4 (-18.6)	7.3%	19.7	1.05×	10.0 (-32.0)	123.5 (-132.5)	51.8%	41.6	2.02×
	SlowFast (Wei et al., 2026)	21.0 (-14.0)	70.0 (-186.0)	72.7%	70.2	3.72×	11.0 (-31.0)	96.8 (-159.2)	62.2%	62.6	3.04×
	KLASS (Kim et al., 2025)	35.0 (+0.0)	109.7 (-146.3)	57.1%	34.0	1.81×	10.0 (-32.0)	111.7 (-144.3)	56.4%	35.1	1.71×
	WINO (Hong et al., 2026)	34.0 (-1.0)	51.2 (-204.8)	80.0%	77.3	4.15×	–	–	–	–	–
	C^4	37.0 (+2.0)	64.4 (-191.6)	74.8%	67.6	3.59×	45.0 (+3.0)	64.9 (-191.1)	74.6%	82.2	3.98×
Code generation (whole-program answer, execution-graded)											
HumanEval	Baseline	40.2	384.0	0.0%	13.8	1.00×	45.1	384.0	0.0%	14.5	1.00×
(n=164, sequence length=384)	Prophet (Li et al., 2026)	3.0 (-37.2)	124.0 (-260.0)	67.7%	30.9	2.24×	0.6 (-44.5)	29.3 (-354.7)	92.4%	144.2	9.93×
(block=32, 12 blocks)	SchED (Mohamed et al., 2026b)	12.8 (-27.4)	175.7 (-208.3)	54.2%	33.1	2.39×	1.8 (-43.3)	39.3 (-344.7)	89.8%	142.9	9.84×
	SlowFast (Wei et al., 2026)	19.5 (-20.7)	36.3 (-347.7)	90.5%	213.1	15.42×	23.2 (-22.0)	36.4 (-347.6)	90.5%	205.6	14.16×
	KLASS (Kim et al., 2025)	40.9 (+0.7)	92.6 (-291.4)	75.9%	45.4	3.29×	25.6 (-19.5)	103.5 (-280.5)	73.0%	34.7	2.39×
	WINO (Hong et al., 2026)	37.8 (-2.4)	54.2 (-329.8)	85.9%	77.0	5.60×	–	–	–	–	–
	C^4	42.1 (+1.9)	39.4 (-344.6)	89.7%	120.0	8.69×	43.3 (-1.8)	29.2 (-354.8)	92.4%	146.0	10.04×
MBPP	Baseline	45.9	384.0	0.0%	15.4	1.00×	56.0	384.0	0.0%	15.6	1.00×
(n=257, sequence length=384)	Prophet (Li et al., 2026)	1.9 (-44.0)	32.1 (-351.9)	91.6%	73.2	4.78×	0.8 (-55.2)	1.4 (-382.6)	99.6%	433.7	27.82×
(block=32, 12 blocks)	SchED (Mohamed et al., 2026b)	27.6 (-18.3)	66.6 (-317.4)	82.7%	101.3	6.60×	1.9 (-54.1)	16.3 (-367.7)	95.8%	414.1	26.54×
	SlowFast (Wei et al., 2026)	41.2 (-4.7)	21.6 (-362.4)	94.4%	362.0	23.62×	46.7 (-9.3)	30.0 (-354.0)	92.2%	274.1	17.58×
	KLASS (Kim et al., 2025)	46.5 (+0.6)	69.2 (-314.8)	82.0%	66.8	4.35×	53.0 (-3.0)	93.1 (-290.9)	75.8%	42.3	2.71×
	WINO (Hong et al., 2026)	47.1 (+1.2)	54.4 (-329.6)	85.8%	88.0	5.79×	–	–	–	–	–
	C^4	45.9 (+0.0)	33.3 (-350.7)	91.3%	170.8	11.11×	56.0 (+0.0)	25.5 (-358.5)	93.4%	209.3	13.42×

Table 1: Zero-shot evaluation under free-form generation. C^4 uses one frozen setting everywhere; each peer keeps its own, which for several differs by task family. Red marks a drop past the 2.0-point tolerance, and it concentrates in the long-reasoning and code panels.

Hyperparameters and calibration. CVEE's tuple (γ=2.0, τ_{CVEE}=0.7, $p_{\min}$=3), SchED's decay schedule, and KLASS's $\tau/\epsilon_{\text{KL}}$ are calibrated once offline on LLaDA using a shared 120-trajectory pool, then reused unchanged for Dream and the remaining nine tasks; Prophet keeps its published defaults. CCTC's τ_{CCTC}=0.8 and hole tolerance H=1 are fixed *a priori* instead: a sampling rule changes which future steps execute, so offline replay cannot faithfully calibrate it, while calibrating it live would tune against the test. Appendix G.2 varies H without per-task selection and treats H=1 only as a fixed within-sweep reference, not as a task-wise optimum. The appendix gives the per-task settings, grading rules, timing protocol, paired statistics, and ablations.

Evaluation metrics and protocol fairness. Accuracy and Step follow Prophet's evaluation convention, exact match after task-specific answer extraction and the number of decoding steps, respectively.

Saving restates Step as the fraction of the full step budget removed, $1 - \text{Step}/T_{\text{full}}$, which makes a 256-step task and a 384-step one comparable at a glance. Speedup is method TPS over baseline TPS. Paired McNemar tests and bootstrap confidence intervals detect no statistically significant accuracy difference between C^4 and Baseline in any cell.

5.1 Main Results and Analysis

Table 1 reports complete zero-shot decoding on examples never used for calibration, across all 12 tasks and both models, with C^4 always deployed as CVEE plus CCTC. Figure 5 places each commit against the step at which that trajectory's answer stopped changing, so anything under a diagonal was premature. One frozen configuration is sufficient throughout, but the source of the step and TPS gains changes sharply by regime.

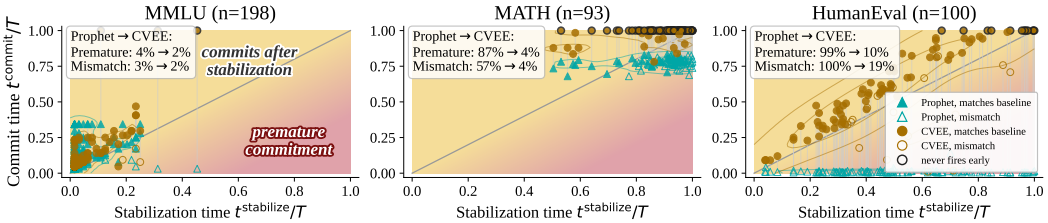

Figure 5: Commit-stabilization phase diagram. Each faint line pairs the Prophet triangle with the CVEE circle on one LLaDA-8B-Instruct evaluation trajectory, so the two are judged on the same run rather than sampled separately. On MMLU both sit on the diagonal. On MATH and HumanEval Prophet drops below it almost everywhere and CVEE does not. A margin-based gate does not fail by a little on hard tasks, it commits before there is an answer to commit to.

Short-answer tasks. CVEE carries this regime almost alone. On MMLU and ARC-C, C^4 uses only 4.8 and 3.9 steps on LLaDA, so the candidate usually settles inside the first block and leaves CCTC little to accelerate. What separates the methods is therefore the quantity each one tests. The termination gates use a position-level margin that keeps moving after the answer has stopped changing, which is why Figure 5 puts them below the diagonal while CVEE stays on it; the samplers measure nothing about an answer, so there is none for them to stop on, and even WINO still spends most of the budget after the answer is fixed. TPS therefore peaks in this regime, where CVEE often removes nearly the whole run rather than merely thinning later blocks.

Long-reasoning tasks. Here the pattern reverses: the candidate settles only near the horizon, so CVEE usually declines to fire and CCTC supplies nearly all the saving by accelerating blocks that must be decoded anyway. Dream GSM8K makes the split explicit: CVEE alone barely leaves the full budget at all, while full C^4 falls to 54.5 steps through CCTC. The lower TPS here reflects the same constraint: many blocks still execute, so wall-clock gains rise less than they do on short-answer tasks even when many step slots disappear. It also shifts the risk. With no exit to get wrong, what remains is whether a step commits the wrong positions. C^4 moves little either way, while WINO swings hard in both, the signature of revocation, which recovers some premature commits and entrenches others. The termination gates, still keyed to their margin, exceed the tolerance everywhere.

Code generation. Here the two gates share the work because the two quantities they test come apart. Structure resolves early even when total length does not, so CVEE contributes again while CCTC accelerates what remains, and the saving returns to the short-answer band despite much longer sequences. On HumanEval, for example, C^4 reaches 42.1 at 39.4 steps on LLaDA, outperforming full decoding while using only 10.3% of the budget. Execution grading makes one wrong token cost the example, so this regime stresses the commit rule rather than the exit. Across the three regimes the two gates never carry the same share twice, and neither is redundant.

5.2 Efficiency Decomposition and Component Ablation

The two axes dominate in different regimes. Table 2 builds the deployed configuration one rung at a time, and the contrast appears immediately: confidence alone collapses on HumanEval (4.9% against 40.2), while stability alone collapses on GSM8K (33.0 against 67.0). The benefit of CCTC

is different: it reduces the step budget inside blocks that still have to be decoded, and its confirm stage recovers the accuracy that a core-only rule can leave behind. CVEE contributes most on the short-answer task shown, CCTC most on GSM8K and HumanEval, and the TPS columns show the same split in wall-clock terms. The full configuration exceeds either component alone in every row, so the two axes compose rather than compete.

		LLaDA-8B-Instruct					Dream-7B-Instruct				
Task	Variant	Acc (%)	Step	Saving	TPS	Speedup	Acc (%)	Step	Saving	TPS	Speedup
General / short-answer tasks											
MMLU (n=200, sequence length=64) (block=16, 4 blocks)	Baseline	64.0	64.0	0.0%	30.4	1.00×	71.5	64.0	0.0%	28.2	1.00×
	+ confidence gate only	64.0	3.7	94.1%	636.8	20.88×	70.5	2.9	95.5%	277.2	9.87×
	+ stability gate only	62.0	4.0	93.7%	525.7	17.18×	70.0	3.7	94.2%	417.0	14.84×
	+ CVEE (joint gate)	64.0	7.0	89.1%	452.7	14.80×	69.5	8.0	87.5%	208.9	7.44×
	+ CCTC, core only	63.5	5.2	91.9%	496.1	16.27×	70.5	5.2	91.9%	323.3	11.54×
	+ CCTC, core then confirm	64.0	5.0	92.1%	491.1	16.10×	70.0	4.7	92.6%	386.4	13.75×
	C^4: CCTC on every block	64.0	4.8	92.5%	490.4	16.16×	70.0	4.5	93.0%	389.7	13.82×
Long-reasoning tasks (multi-step CoT)											
GSM8K (n=100, sequence length=256) (block=32, 8 blocks)	Baseline	66.0	256.0	0.0%	19.0	1.00×	85.0	256.0	0.0%	21.2	1.00×
	+ confidence gate only	61.0	59.2	76.9%	20.7	1.09×	83.0	53.8	79.0%	21.3	1.01×
	+ stability gate only	33.0	24.5	90.4%	50.0	2.63×	83.0	53.2	79.2%	23.3	1.10×
	+ CVEE (joint gate)	66.0	250.0	2.3%	19.2	1.01×	85.0	256.0	0.0%	21.1	1.00×
	+ CCTC, core only	66.0	85.2	66.7%	51.8	2.72×	85.0	85.8	66.5%	63.7	3.01×
	+ CCTC, core then confirm	66.0	83.9	67.2%	52.0	2.73×	85.0	84.3	67.1%	64.6	3.05×
	C^4: CCTC on every block	64.0	62.5	75.6%	67.5	3.55×	85.0	54.5	78.7%	102.1	4.82×
Code generation (whole-program answer)											
HumanEval (n=164, sequence length=384) (block=32, 12 blocks)	Baseline	40.2	384.0	0.0%	13.8	1.00×	45.1	384.0	0.0%	14.5	1.00×
	+ confidence gate only	4.9	9.7	97.5%	67.6	4.89×	5.5	9.5	97.5%	196.5	13.53×
	+ stability gate only	42.1	39.4	89.7%	24.8	1.79×	43.3	29.2	92.4%	43.9	3.02×
	+ CVEE (joint gate)	37.2	212.4	44.7%	24.8	1.79×	42.7	109.2	71.6%	39.3	2.70×
	+ CCTC, core only	40.9	50.0	87.0%	90.8	6.57×	43.3	36.6	90.5%	116.5	8.02×
	+ CCTC, core then confirm	42.1	48.8	87.3%	92.6	6.70×	43.3	35.8	90.7%	119.0	8.19×
	C^4: CCTC on every block	42.1	39.4	89.7%	120.0	8.69×	43.3	29.2	92.4%	146.0	10.04×

Table 2: Component ablation. Core only commits the boundary-anchored core; core then confirm adds the round confirming what it withheld; the last row accelerates every block and is the deployed system. CVEE drives short-answer speedup and CCTC the rest, and Dream's GSM8K barely leaves the full budget under CVEE alone, rarely offering a late extractable candidate.

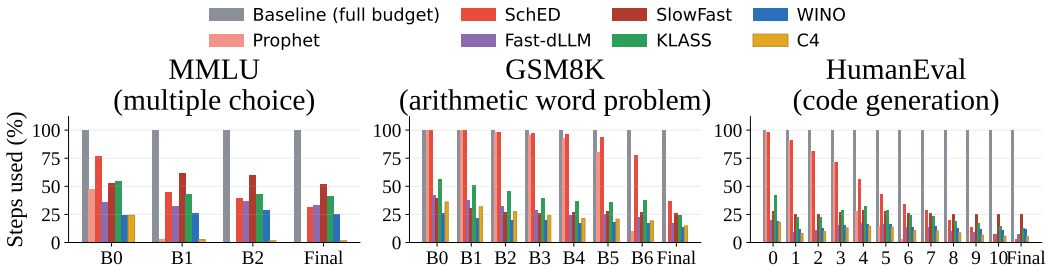

Figure 6: Per-block step usage. Mean steps used (% of per-block budget), LLaDA-8B-Instruct.

Per-block step usage shows where CCTC helps and where CVEE has little left to do. Figure 6 shows where the budget actually goes. No block is exempt now, so none stays at full budget. On GSM8K, usage falls from about a third of the allowance in the first block to about a sixth in the last; on HumanEval, every block after the first sits below a fifth. What remains is a floor rather than a single bottleneck, which helps explain why long-reasoning speedups plateau where code's do not. Shortanswer tasks instead finish inside one block and spend almost nothing on the rest, which is why CVEE carries most of the gain there and CCTC has little left to remove. The measured throughput matches that picture: no long-reasoning speedup exceeds 6.32×, every code speedup is at least 8.69×, and the short-answer tasks all clear 13×.

6 Conclusion

Semi-autoregressive decoding leaves two decisions open: which token positions a step may commit and when the sequence may stop. C^4 answers them with two gates matched to those two scopes: CCTC governs block-local commitment by keeping an autoregressive freezing order inside each block, while CVEE governs global termination by verifying the extracted candidate answer itself before the remaining buffer is filled. Across 12 tasks and two backbones under one frozen gate configuration, it removes 64–95% of the decoding steps and delivers measured end-to-end speedups of 2.6× to 18.6×. This coordination works only if each gate verifies the object appropriate to its own scope. Token-level confidence can guide local commitment, whereas sequence termination must verify the candidate answer itself. In the present form that verification assumes a format-delimited answer unit, leaving open-ended generation as the main frontier for future work.

References

Jacob Austin, Daniel D Johnson, Jonathan Ho, Daniel Tarlow, and Rianne Van Den Berg. Structured denoising diffusion models in discrete state-spaces. *Advances in Neural Information Processing Systems (NeurIPS)*, 34:17981–17993, 2021a.

Jacob Austin, Augustus Odena, Maxwell Nye, Maarten Bosma, Henryk Michalewski, David Dohan, Ellen Jiang, Carrie Cai, Michael Terry, Quoc Le, and Charles Sutton. Program synthesis with large language models. *arXiv preprint arXiv:2108.07732*, 2021b.

Yonatan Bisk, Rowan Zellers, Ronan Le Bras, Jianfeng Gao, and Yejin Choi. PIQA: Reasoning about physical commonsense in natural language. In *Proceedings of the AAAI Conference on Artificial Intelligence (AAAI)*, 2020.

Andrew Campbell, Joe Benton, Valentin De Bortoli, Thomas Rainforth, George Deligiannidis, and Arnaud Doucet. A continuous time framework for discrete denoising models. *Advances in Neural Information Processing Systems (NeurIPS)*, 35:28266–28279, 2022.

Mark Chen, Jerry Tworek, Heewoo Jun, Qiming Yuan, Henrique Ponde de Oliveira Pinto, Jared Kaplan, Harri Edwards, Yuri Burda, Nicholas Joseph, Greg Brockman, et al. Evaluating large language models trained on code. *arXiv preprint arXiv:2107.03374*, 2021.

Xinhua Chen, Sitao Huang, Cong Guo, Chiyue Wei, Yintao He, Jianyi Zhang, Hai Li, and Yiran Chen. DPad: Efficient diffusion language models with suffix dropout. *arXiv preprint arXiv:2508.14148*, 2025. URL https://arxiv.org/abs/2508.14148.

Yuzhe Chen, Jiale Cao, Xuyang Liu, Jin Xie, Aiping Yang, and Yanwei Pang. STDec: Spatio-temporal stability guided decoding for dLLMs. *arXiv preprint arXiv:2604.06330*, 2026.

Peter Clark, Isaac Cowhey, Oren Etzioni, Tushar Khot, Ashish Sabharwal, Carissa Schoenick, and Oyvind Tafjord. Think you have solved question answering? try ARC, the AI2 reasoning challenge. *arXiv preprint arXiv:1803.05457*, 2018.

Karl Cobbe, Vineet Kosaraju, Mohammad Bavarian, Mark Chen, Heewoo Jun, Lukasz Kaiser, Matthias Plappert, Jerry Tworek, Jacob Hilton, Reiichiro Nakano, et al. Training verifiers to solve math word problems. *arXiv preprint arXiv:2110.14168*, 2021. URL https://arxiv.org/abs/2110.14168.

Muzhi Dai, Chenxu Yang, and Qingyi Si. S-GRPO: Early exit via reinforcement learning in reasoning models. In *Advances in Neural Information Processing Systems 38 (NeurIPS)*, 2025. URL https://openreview.net/forum?id=wNMK5o0Vfg.

Justin Deschenaux and Caglar Gulcehre. Beyond autoregression: Fast LLMs via self-distillation through time. In *International Conference on Learning Representations (ICLR)*, 2025. URL https://arxiv.org/abs/2410.21035.

Zhenbang Du, Kejing Xia, Xinrui Zhong, Yonggan Fu, Nicolai Oswald, Binfei Ji, Brucek Khailany, Pavlo Molchanov, and Yingyan Lin. R^2-dLLM: Accelerating diffusion large language models via spatio-temporal redundancy reduction. *arXiv preprint arXiv:2604.18995*, 2026.

Luyu Gao, Aman Madaan, Shuyan Zhou, Uri Alon, Pengfei Liu, Yiming Yang, Jamie Callan, and Graham Neubig. PAL: Program-aided language models. *International Conference on Machine Learning (ICML)*, 2023.

Jiawei Gu, Ziyue Qiao, and Xiao Luo. Detecting the semantic fixed point: A geometric framework for efficient inference. In *Proceedings of the 43rd International Conference on Machine Learning (ICML)*, 2026. URL https://openreview.net/forum?id=DACN5xM4h7.

Dan Hendrycks, Collin Burns, Steven Basart, Andy Zou, Mantas Mazeika, Dawn Song, and Jacob Steinhardt. Measuring massive multitask language understanding. In *International Conference on Learning Representations (ICLR)*, 2021a.

Dan Hendrycks, Collin Burns, Saurav Kadavath, Akul Arora, Steven Basart, Eric Tang, Dawn Song, and Jacob Steinhardt. Measuring mathematical problem solving with the MATH dataset. In *NeurIPS Datasets and Benchmarks Track (NeurIPS)*, 2021b.

Feng Hong et al. Wide-in, narrow-out: Revokable decoding for efficient and effective DLLMs. In *International Conference on Learning Representations (ICLR)*, 2026. URL https://openreview.net/pdf?id=XtLQHlNLxy.

Emiel Hoogeboom, Didrik Nielsen, Priyank Jaini, Patrick Forré, and Max Welling. Argmax flows and multinomial diffusion: Learning categorical distributions. *Advances in Neural Information Processing Systems (NeurIPS)*, 34:12454–12465, 2021.

Jiyeon Kim, Sungik Choi, Yongrae Jo, Moontae Lee, and Minjoon Seo. Early decisions matter: Proximity bias and initial trajectory shaping in non-autoregressive diffusion language models. *arXiv preprint arXiv:2604.10567*, 2026. URL https://arxiv.org/abs/2604.10567.

Seo Hyun Kim, Sunwoo Hong, Hojung Jung, Youngrok Park, and Se-Young Yun. KLASS: KL-guided fast inference in masked diffusion models. In *Advances in Neural Information Processing Systems 38 (NeurIPS), Spotlight*, 2025. arXiv:2511.05664.

Jungseob Lee, Seongtae Hong, Seungjun Lee, Jaehyung Seo, Junyoung Son, Sugyeong Eo, Chanjun Park, Hyeongju Park, Hyeonseok Moon, and Heuiseok Lim. DART: Draft-agreement routing for training-free adaptive thinking budgets in hybrid reasoning models. *arXiv preprint arXiv:2606.23181*, 2026. URL https://arxiv.org/abs/2606.23181.

Pengxiang Li, Yefan Zhou, Dilxat Muhtar, Lu Yin, Shilin Yan, Li Shen, Yi Liang, Soroush Vosoughi, and Shiwei Liu. Diffusion language model knows the answer before it decodes. In *The Fourteenth International Conference on Learning Representations (ICLR)*, 2026. URL https://openreview.net/forum?id=g88nt4ieTG.

Aaron Lou, Chenlin Meng, and Stefano Ermon. Discrete diffusion modeling by estimating the ratios of the data distribution. In *Proceedings of the 41st International Conference on Machine Learning (ICML)*, volume 235 of *Proceedings of Machine Learning Research*, pp. 32819–32848, 2024. URL https://proceedings.mlr.press/v235/lou24a.html.

Shen-Yun Miao, Chao-Chun Liang, and Keh-Yih Su. A diverse corpus for evaluating and developing English math word problem solvers. In *Proceedings of the 58th Annual Meeting of the Association for Computational Linguistics (ACL)*, 2020.

Amr Mohamed, Guokan Shang, and Michalis Vazirgiannis. LESS is more: Mutual-stability sampling for diffusion language models. *arXiv preprint arXiv:2606.16908*, 2026a. URL https://arxiv.org/abs/2606.16908.

Amr Mohamed, Yang Zhang, Michalis Vazirgiannis, and Guokan Shang. Fast-decoding diffusion language models via progress-aware confidence schedules. In *Findings of the Association for Computational Linguistics: ACL 2026*, 2026b. arXiv:2512.02892.

Shen Nie, Fengqi Zhu, Zebin You, Xiaolu Zhang, Jingyang Ou, Jun Hu, Jun Zhou, Yankai Lin, Ji-Rong Wen, and Chongxuan Li. Large language diffusion models. In *Advances in Neural Information Processing Systems 38 (NeurIPS)*, 2025. URL https://openreview.net/forum?id=KnqiC0znVF. arXiv:2502.09992.

Jingyang Ou, Shen Nie, Kaiwen Xue, Fengqi Zhu, Jiacheng Sun, Zhenguo Li, and Chongxuan Li. Your absorbing discrete diffusion secretly models the conditional distributions of clean data. In *The Thirteenth International Conference on Learning Representations (ICLR)*, 2025. URL https://openreview.net/forum?id=sMyXP8Tanm.

Arkil Patel, Satwik Bhattamishra, and Navin Goyal. Are NLP models really able to solve simple math word problems? In *Proceedings of the 2021 Conference of the North American Chapter of the Association for Computational Linguistics (NAACL)*, 2021.

Jiaoyang Ruan, Xin Gao, Yinda Chen, Hengyu Zeng, Liang Du, Guanghao Li, Jie Fu, and Jian Pu. Reasoning on the manifold: Bidirectional consistency for self-verification in diffusion language models. In *Proceedings of the 43rd International Conference on Machine Learning (ICML)*, 2026. URL https://openreview.net/forum?id=CUVBdw2tKy. arXiv:2604.16565.

Subham Sekhar Sahoo, Marianne Arriola, Yair Schiff, Aaron Gokaslan, Edgar Marroquin, Justin T. Chiu, Alexander Rush, and Volodymyr Kuleshov. Simple and effective masked diffusion language models. In *Advances in Neural Information Processing Systems 37 (NeurIPS)*, 2024. URL https://proceedings.neurips.cc/paper_files/paper/2024/hash/eb0b13cc515724ab8015bc978fdde0ad-Abstract-Conference.html.

Keisuke Sakaguchi, Ronan Le Bras, Chandra Bhagavatula, and Yejin Choi. WinoGrande: An adversarial Winograd schema challenge at scale. *Communications of the ACM*, 64(9):99–106, 2021.

Jiaxin Shi, Kehang Han, Zhe Wang, Arnaud Doucet, and Michalis K. Titsias. Simplified and generalized masked diffusion for discrete data. In *Advances in Neural Information Processing Systems 37 (NeurIPS)*, 2024. URL https://proceedings.neurips.cc/paper_files/paper/2024/hash/bad233b9849f019aead5e5cc60cef70f-Abstract-Conference.html.

Jascha Sohl-Dickstein, Eric Weiss, Niru Maheswaranathan, and Surya Ganguli. Deep unsupervised learning using nonequilibrium thermodynamics. In *International Conference on Machine Learning (ICML)*, pp. 2256–2265, 2015.

Chengcheng Wang, Tingzhang Luo, Wenhao Li, Jianyuan Guo, and Chang Xu. TACG: Trajectory-aware commit gating for diffusion language model decoding. *arXiv preprint arXiv:2607.03236*, 2026.

Qingyan Wei, Yaojie Zhang, Zhiyuan Liu, Puyu Zeng, Yuxuan Wang, Biqing Qi, Dongrui Liu, and Linfeng Zhang. Accelerating diffusion large language models with SlowFast sampling: The three golden principles. In *The Fourteenth International Conference on Learning Representations (ICLR)*, 2026. URL https://openreview.net/forum?id=Uh17FiwF4q. arXiv:2506.10848.

Chengyue Wu, Hao Zhang, Shuchen Xue, Zhijian Liu, Shizhe Diao, Ligeng Zhu, Ping Luo, Song Han, and Enze Xie. Fast-dLLM: Training-free acceleration of diffusion LLM by enabling KV cache and parallel decoding. In *The Fourteenth International Conference on Learning Representations (ICLR)*, 2026. URL https://openreview.net/forum?id=3Z3Is6hnOT. arXiv:2505.22618.

Andrea Wynn, Metod Jazbec, Charith Peris, Rinat Khaziev, Anqi Liu, Daniel Khashabi, and Eric Nalisnick. Controlling the risk of corrupted contexts for language models via early-exiting. In *Proceedings of the 43rd International Conference on Machine Learning (ICML)*, 2026. URL https://openreview.net/forum?id=8bUDbWMo5v. arXiv:2510.02480.

Yangxinyu Xie, Tao Wang, Soham Mallick, Yan Sun, Georgy Noarov, Mengxin Yu, Tanwi Mallick, Weijie J. Su, and Edgar Dobriban. Statistical early stopping for reasoning models. In *Proceedings of the 43rd International Conference on Machine Learning (ICML)*, 2026. URL https://openreview.net/forum?id=TJshRZDdyW. arXiv:2602.13935.

Chenxu Yang, Qingyi Si, Yongjie Duan, Zheliang Zhu, Chenyu Zhu, Qiaowei Li, Minghui Chen, Zheng Lin, and Weiping Wang. Dynamic early exit in reasoning models. In *The Fourteenth International Conference on Learning Representations (ICLR)*, 2026. URL https://openreview.net/forum?id=NpU7ZXafRi.

Jiacheng Ye, Zhihui Xie, Lin Zheng, Jiahui Gao, Zirui Wu, Xin Jiang, Zhenguo Li, and Lingpeng Kong. Dream 7B: Diffusion large language models. *arXiv preprint arXiv:2508.15487*, 2025. URL https://arxiv.org/abs/2508.15487.

Rowan Zellers, Ari Holtzman, Yonatan Bisk, Ali Farhadi, and Yejin Choi. HellaSwag: Can a machine really finish your sentence? In *Proceedings of the 57th Annual Meeting of the Association for Computational Linguistics (ACL)*, 2019.

Kevin Zhai, Sabbir Mollah, Zhenyi Wang, and Mubarak Shah. CORE: Context-robust remasking for diffusion language models. In *Proceedings of the 43rd International Conference on Machine Learning (ICML)*, 2026. URL https://openreview.net/forum?id=bmKHxLWkz9. arXiv:2602.04096.

Yu Zhang, Xinchen Li, Jialei Zhou, Hongnan Ma, Zhongwei Wan, Yiwei Shi, Duoqian Miao, Qi Zhang, and Longbing Cao. Swordsman: Entropy-driven adaptive block partition for efficient diffusion language models. In *Proceedings of the 43rd International Conference on Machine Learning (ICML)*, 2026. arXiv:2602.04399.

Haoyang Zheng, Xinyang Liu, Cindy Xiangrui Kong, Nan Jiang, Zheyuan Hu, Weijian Luo, Wei Deng, and Guang Lin. Ultra-fast language generation via discrete diffusion divergence instruct. In *International Conference on Learning Representations (ICLR)*, 2026.

Kaiwen Zheng, Yongxin Chen, Hanzi Mao, Ming-Yu Liu, Jun Zhu, and Qinsheng Zhang. Masked diffusion models are secretly time-agnostic masked models and exploit inaccurate categorical sampling. In *The Thirteenth International Conference on Learning Representations (ICLR)*, 2025. URL https://openreview.net/forum?id=CTC7CmirNr.

Appendix Overview

Grouped by theme. Appendices A–C cover reproducibility, protocol and statistical validation, Appendix D covers mechanistic analysis and fairness, Appendices E–G scaling and sensitivity, and Appendix H limitations.

- **A** Hyperparameters and harness details.
- **B** Timing protocol.
- **C** Paired significance and output-identical rate.
- **D** Mechanistic failure case.
- **E** Scaling and composition.
- **F** Composing CVEE with a third-party sampler.
- **G** Sensitivity.
- **H** Limitations.

A Hyperparameters Underlying Table 1

A.1 Harness Details and the Deployed Configuration

Harness details deferred from Section 5. Zero-shot means a bare question plus, for reasoning tasks, a one-line "Let's think step by step" CoT cue, with no exemplars and no answer-format scaffolding beyond that. Dream-7B-Instruct retains a causal-LM next-token indexing convention; our harness applies its own official one-position logit shift, otherwise decoding matches LLaDA. The Prophet peer row ports the official gate (unchanged published defaults) into this same harness, monitoring our own answer region, rather than citing numbers from Prophet's own repo, which uses a different prompt template.

Table 1's central claim is that C^4 needs exactly one *numerical* hyperparameter configuration, τ_{CVEE}=0.7, γ=2.0 and $p_{\min}$=3 of Eq. 4, τ_{CCTC}=0.8 and hole tolerance H=1 of Eq. 6, `tail_frac`=0.3 of Section 4, identical across all 12 tasks and both models, with no per-task or per-model retuning (the deterministic extractor and search region follow each task's own output format, `search_mode` below, but neither is tuned). Table 3 makes this explicit alongside the one setting that *does* vary by task, Prophet's own staged confidence-gap thresholds, which vary by task family as Section 5 notes. That is exactly the per-task tuning C^4 is designed to avoid needing.

Task	n	len	Steps	Block	search_mode	Prophet ($\tau_{\text{high}}/\tau_{\text{mid}}/\tau_{\text{low}}$)	SchED (mode/patience)	KLASS ($\tau/\epsilon_{\text{KL}}$)	WINO (τ/τ_{back})
MMLU	200	64	64	16	first5	7.5 / 5.0 / 2.5	cosine / 0	0.7 / 0.015	0.5 / 0.9
ARC-C	200	64	64	16	first5	7.5 / 5.0 / 2.5	cosine / 0	0.7 / 0.015	0.5 / 0.9
HellaSwag	200	64	64	16	first5	7.5 / 5.0 / 2.5	cosine / 0	0.7 / 0.015	0.5 / 0.9
WinoGrande	200	64	64	16	first5	7.5 / 5.0 / 2.5	cosine / 0	0.7 / 0.015	0.5 / 0.9
PIQA	200	64	64	16	first5	7.5 / 5.0 / 2.5	cosine / 0	0.7 / 0.015	0.5 / 0.9
GSM8K	100	256	256	32	last	8.0 / 5.0 / 3.5	linear / 4	0.6 / 0.015	0.6 / 0.9
MATH	100	256	256	32	last	8.0 / 5.0 / 3.5	linear / 4	0.6 / 0.015	0.7 / 0.9
SVAMP	100	256	256	32	last	8.0 / 5.0 / 3.5	linear / 4	0.6 / 0.015	0.6 / 0.9
ASDiv	100	256	256	32	last	8.0 / 5.0 / 3.5	linear / 4	0.6 / 0.015	0.6 / 0.9
GSM-Hard	100	256	256	32	last	8.0 / 5.0 / 3.5	linear / 4	0.6 / 0.015	0.6 / 0.9
HumanEval	164	384	384	32	code	7.5 / 5.0 / 4.5	cosine / 4	0.9 / 0.01	0.7 / 0.9
MBPP	257	384	384	32	code	7.5 / 5.0 / 4.5	cosine / 4	0.7 / 0.01	0.8 / 0.9

Table 3: Per-task settings underlying Table 1. n is the evaluation sample size; len is generation length; Steps is the full decode budget; Block is the block-diffusion block size. `search_mode` is fixed by answer format, never tuned. Each peer's column is explained below.

C^4. Its five hyperparameters are identical on every row, listed above, and are not shown per task because there is nothing per task to show.

Prophet. Its staged thresholds are taken unchanged from its own paper and repository, not tuned by us. The code rows differ from the other two families because its own appendix publishes a separate code-generation schedule (7.5/5.0/4.5).

SchED. Mode and patience are its calibrated decay-curve shape and stability-guard patience; $\tau_{\text{high}}/\tau_{\text{low}}$ reuse Prophet's values above. It publishes no code-generation configuration, so we ran both its paper default and that default plus its long-form stability guard, and report the guarded run, which scored higher on both backbones (12.8 against 9.8 on LLaDA, 1.8 against 0.6 on Dream).

KLASS. $\tau/\epsilon_{\text{KL}}$ are its two frozen-per-family calibrated values, except on the code rows, where it ships per-task scripts of its own and those are used verbatim: 0.9 / 0.01 on LLaDA and 0.8 / 0.001 on Dream for HumanEval, 0.7 / 0.01 and 0.9 / 0.001 for MBPP.

WINO. Its column is the published threshold wherever it publishes one (ARC-Challenge, GSM8K, MATH, HumanEval, MBPP) and its nearest published family's value otherwise, the same per-family freezing applied to SchED; τ_{back} is 0.9 in every configuration it releases.

Everything else. Remaining hyperparameters of both peers and of C^4 are fixed across rows and are not reproduced here.

	Prophet	SchED	SlowFast	KLASS	C^4
LLaDA (wall-clock)	–	57m	–	2h50m	3h43m
GPU-free?	–	✓	–	×	×
Transfers to Dream?	×	×	×	×	✓

Table 4: Calibration wall-clock time, discussed in Section 5.2. "–" denotes no separate calibration (hyperparameters are published or inherited). GPU-free: ✓ offline, × needs GPU. Transfers to Dream: ✓ holds, × fails.

A.2 What `search_mode` Controls

`search_mode` fixes, per task family, which region of the buffer the extractor scans and where the gate relocates the answer span, never tuned. `"last"` (GSM8K, MATH, SVAMP, ASDiv, GSM-Hard) restricts both to the trailing `tail_frac`=0.3 fraction; `"first5"` (MMLU, ARC-C, HellaSwag, WinoGrande, PIQA, TruthfulQA) scans the whole buffer but restricts the search to the first 5 positions. `"code"` (HumanEval) scans the whole buffer as well and takes the span running from the buffer's start through the end of the generated function's body, which Python's indentation structure marks at the first non-blank line returning to column zero. The span is located in character space and mapped back to token indices, since a detokenize-and-retokenize round trip does not preserve the token boundaries of an indented multi-line body the way it does for a number or a letter.

A.3 Extractor Normalization, Missing Candidates, and Confidence Aggregation

The change-tracking comparison in Eq. 4 uses the extractor's own normalized output, never a raw token span. Numeric answers have currency symbols and punctuation stripped, boxed math answers have LaTeX spacing/macros canonicalized, so formatting changes and span movement never register as a change; only the normalized value is compared.

run_t is an implementation-maintained stability counter, not a step count; it increments across successive valid extractions with the same value and pauses, rather than resets, when no candidate is extractable (changes_t likewise holds; c_t is undefined, failing the gate automatically). Across 120 calibration trajectories, 30% show such a gap and 21% show the counter resuming through it; a strict-restart-at-one counterfactual reproduces the same commit outcome everywhere, so resumption is common but never decision-changing.

On HumanEval the same rule carries one consequence worth stating explicitly. A function span can reach past the block the schedule is currently decoding, and confidence is undefined by construction at positions no block has begun, so those steps count as having no extractable candidate and leave both counters untouched. Treating them instead as valid observations would let the provisional text at undecoded positions register hundreds of spurious changes before the first meaningful one, which γ would then convert into an unreachable stability requirement. Scalar-answer tasks get the same protection for free, since an extractor finds no number or letter in a region that has not been decoded yet.

Confidence c_t is the model's per-step softmax mean over the span, recomputed each step regardless of mask status, so it may partly reflect self-reconstruction rather than genuine uncertainty; we treat it as an operational agreement score, not an epistemic estimate. We use the plain mean rather than a minimum or geometric mean to avoid penalizing longer answers, though run_t's joint requirement limits how much one lucky token can do alone.

B Timing Protocol

Every displayed TPS/Speedup number in this paper is timed **directly, end-to-end**, not extrapolated from a shared per-step constant. For every cell we wrap one complete call to the decode loop (full step-by-step decoding, CVEE/CCTC gate bookkeeping including the per-step answer-stability extractor, and the final-fill commit when the gate stops early) in `torch.cuda.synchronize()` immediately before/after, timed on the host with `time.time()` (wall clock, not a CUDA event timer). This applies uniformly to *Baseline*, *Prophet*, C^4, *SlowFast Sampling* (Wei et al., 2026), *SchED* (Mohamed et al., 2026b), and *KLASS* (Kim et al., 2025) in Table 1, with the same rule applied to the ablation and scaling cells and to the aggregate labels in the TPS figures.

Protocol. Every cell uses the identical, fixed n=20 subsample, the first 20 of the same evaluation examples Table 1 uses, at `seed`=0 and `skip`=40 for all timing within that cell. 2 warmup examples (a disjoint, immediately-following slice) are decoded and discarded first to absorb first-call overhead (CUDA context/kernel warmup), then 3 timed passes run back to back over the same 20 examples; we report the mean of the 3 pass-level means, plus their coefficient of variation (CV%), so no cell's number rests on a single run. Every cell runs on a GPU with no other job co-resident, verified before launch as Table 5 records, batch size 1, which matches *Prophet*'s and *SlowFast Sampling*'s own released protocols of Section 5. *SchED* and *KLASS* run under this same fixed batch size for a controlled comparison, since neither paper specifies its own, `bf16`, greedy decoding.

Setting	Value
GPU	NVIDIA GeForce RTX 4090, no co-resident job
Driver	580.173.02
Batch size	1
PyTorch / CUDA	2.5.1+cu121 / 12.1
Sync. method	`torch.cuda.synchronize()` around each timed call; host `time.time()`
n / warmup / repeats	20 / 2 / 3, `seed=0`, `skip=40`
LLaDA per-cell CV%	0.00–2.98% (mean 0.14%, n=234 timed cells)
Dream per-cell CV%	0.00–0.48% (mean 0.08%, n=150 timed cells)

Table 5: Direct end-to-end TPS measurement protocol. Shared by every table/figure in Appendix B's scope. CV% is the coefficient of variation across each cell's 3 timed passes; every timed cell lands under 2.99%, showing the 3-pass mean is stable rather than noise-dominated.

C Paired Significance and Output-Identical Rate

Why the comparison is paired. Table 1 reports point estimates, and the ±2.0-point threshold is a prespecified practical tolerance, not a confidence interval. *Baseline* and C^4 are not independent samples: every example is decoded from the identical prompt, model and seed, so the right comparison is paired, and paired uncertainty is far tighter than a naive independent-sample interval ($\approx$ ±6–7pt at n=100 under a binomial approximation) would suggest.

Three statistics per cell. **Output-identical rate** is the fraction of examples whose extracted answer exactly matches the full-budget decode's — direct confirmation that early commitment did not *change* the answer, independent of whether that answer was correct. **McNemar's exact test** runs on the examples where the two disagree, with b baseline-only-correct and c C^4-only-correct; a symmetric split is consistent with equal accuracy, an asymmetric one is not. The **paired bootstrap** 95% CI on Δacc resamples example indices rather than independent draws.

What the numbers say. Output-identical rate is 88–100% on every task: early commitment overwhelmingly reproduces the exact answer the full-budget decode would have reached, not merely a similarly-accurate different one. The disagreement counts b and c are small everywhere (≤ 3 of

	LLaDA-8B-Instruct						Dream-7B-Instruct					
Task	n	b	c	p	Δacc [95% CI]	Ident.(%)	n	b	c	p	Δacc [95% CI]	Ident.(%)
MMLU	200	1	1	1.000	+0.0 [−1.5, +1.5]	99.0	200	3	0	0.250	−1.5 [−3.5, +0.0]	97.5
ARC-C	200	1	0	1.000	−0.5 [−1.5, +0.0]	99.5	200	1	0	1.000	−0.5 [−1.5, +0.0]	99.5
HellaSwag	200	0	0	1.000	+0.0 [+0.0, +0.0]	99.5	200	0	0	1.000	+0.0 [+0.0, +0.0]	100.0
WinoGrande	200	1	2	1.000	+0.5 [−1.0, +2.5]	98.5	200	0	0	1.000	+0.0 [+0.0, +0.0]	100.0
PIQA	200	2	2	1.000	+0.0 [−2.0, +2.0]	98.0	200	0	0	1.000	+0.0 [+0.0, +0.0]	100.0
TruthfulQA	200	0	0	1.000	+0.0 [+0.0, +0.0]	100.0	200	0	1	1.000	+0.5 [+0.0, +1.5]	99.0
GSM8K	100	1	2	1.000	+1.0 [−2.0, +5.0]	97.0	100	0	0	1.000	+0.0 [+0.0, +0.0]	100.0
MATH	100	1	1	1.000	+0.0 [−3.0, +3.0]	94.0	100	0	0	1.000	+0.0 [+0.0, +0.0]	96.0
SVAMP	100	1	1	1.000	+0.0 [−3.0, +3.0]	98.0	100	1	0	1.000	−1.0 [−3.0, +0.0]	98.0
ASDiv	100	1	1	1.000	+0.0 [−3.0, +3.0]	95.0	100	2	0	0.500	−2.0 [−5.0, +0.0]	97.0
GSM-Hard	100	0	1	1.000	+1.0 [+0.0, +3.0]	88.0	100	1	1	1.000	+0.0 [−3.0, +3.0]	93.0

Table 6: Paired statistics for the accuracy difference in Table 1. For each task and model, b and c denote *Baseline*-only-correct and C^4-only-correct examples in McNemar's exact test; Δacc reports the paired bootstrap point estimate and 95% CI; Ident.(%) is the output-identical rate. No cell reaches conventional significance, and every CI stays near zero.

100–200 examples), which is itself informative but leaves McNemar's exact test with essentially no power at this sample size; no task reaches conventional significance and the smallest p-value is 0.25. The paired bootstrap CI is substantially narrower than the naive binomial SE (≈4.7pt at GSM8K's n=100) and centred at or near zero on every task.

What they do not say. These are not equivalence tests for the ±2.0-point margin. Some intervals reach $[-5.0, +0.0]$ or $[-3.0, +3.0]$, wide enough that they do not themselves certify the margin holds; what they rule out is that the reported differences are a systematic accuracy loss rather than sampling noise.

Interpreting the disagreements. b and c are the *counts* of examples where the two variants land on opposite sides of correct/incorrect; the underlying per-example diffs show these are exactly the kind of noise any two similarly-accurate decodes would produce, not a systematic direction. GSM-Hard/LLaDA's lowest identical rate (consistent with that task's own long floating-point-noisy targets) is still mostly both-wrong on different wrong numbers, not C^4 converting a right answer to a wrong one. Dream/MMLU is the one cell with a one-sided split worth naming (b=3, c=0), still far short of significance (p=0.25) at this sample size, and the paired bootstrap CI's upper bound still touches 0.0, so it does not establish that the drop turns severe, but it is the single most CVEE-unfavorable cell in the whole sweep.

D Mechanistic Failure Case: Prophet vs. C^4 on Real Trajectories

Columns 1 and 3 replay the *same* GSM8K decode, so every intermediate output is identical and the two gates' decisions are directly comparable, one model run, two gate outcomes. All three columns replay the exact deployed hyperparameters (τ_{CVEE}=0.7, γ=2.0, $p_{\min}$=3). Every column shares the same four-panel structure (candidate answer identity, the model's own verification signal, the basis of the eventual commit decision, and the answer-region predictive entropy H_t against decoding progress), so the contrast is legible panel-for-panel.

Prophet (column 1): the correct answer surfaces repeatedly, but nothing locks it in. The candidate hits the correct value, 21, twice in passing before the gate fires at step 139 of 256; Prophet's own top1-top2 logit gap simply has no mechanism to distinguish a passing correct guess from any other transient one. The gap panel shows why the gate fires *anyway*. The gap itself never rises appreciably; it is Prophet's own staged threshold, tuned for this task family, as Appendix A.1 records, that decays until the noisy gap crosses it. At that exact moment the tail window monitored by the gate is 100% masked (row 3); every token in it is force-filled from a single, unrefined forward pass in one shot, and the entropy panel (row 4) shows why that is dangerous; H_t≈0.48 bits of real uncertainty remain in that same window at the instant of commit, not the near-zero value a genuine convergence would show. The one-shot fill lands on a truncated, garbled continuation with no extractable number at all (graded wrong by construction), the same failure mode, corrupted trailing text rather than a clean wrong digit. This is the mechanism behind the 12–69 point collapses in Table 1, not a badly-tuned threshold, but a gate with no way to tell a transient guess from a verified one.

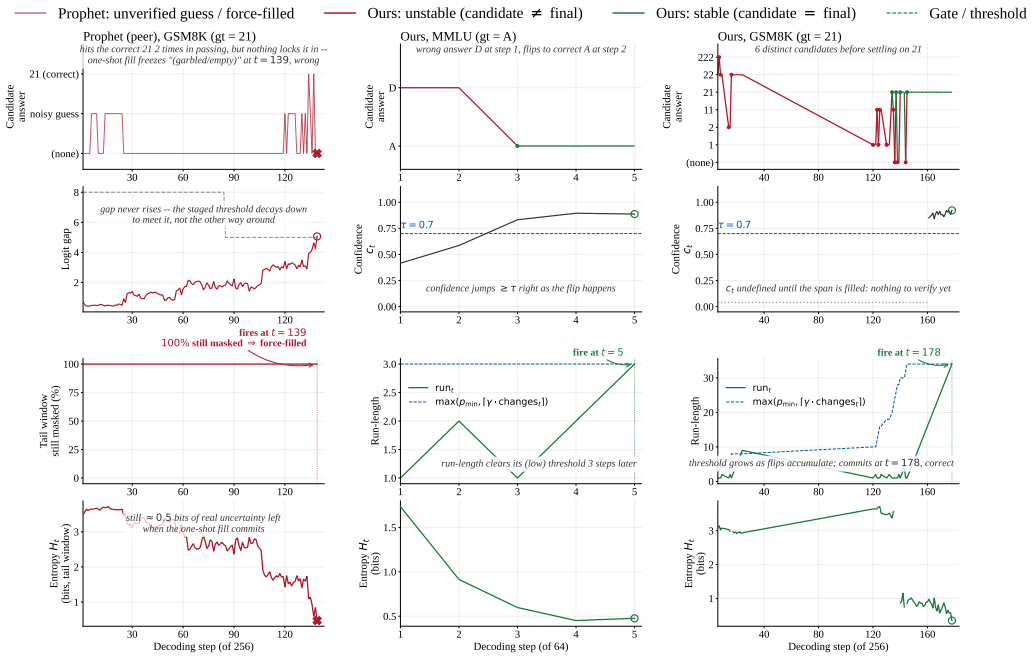

Figure 7: Prophet vs. CVEE on representative trajectories. Why Prophet fails and how Confidence-Verified Early Exit fixes it, on one representative real GSM8K trajectory. Figure 3 pools n=40 such trajectories with bootstrap CIs, so this single example does not carry the paper's claim by itself. Columns 1 and 3 replay the identical trajectory (gt= 21): Prophet commits at 54% progress to a garbled non-answer (100% of its window still masked); ours withholds until 70% and gets it right. Column 2 (MMLU) succeeds after one false start.

C^4 (columns 2–3): the same two mechanisms (confidence and run-length) rule out exactly this failure. On MMLU (column 2), the candidate is wrong (D) at step 1, flips to the correct answer (A) at step 2 with confidence jumping from 0.42 to 0.83 (crossing τ_{CVEE} in the same step as the flip, not gradually), and the gate fires three steps later once the run-length requirement is also satisfied, at step 5 of 64 (8% of budget); entropy over that same span has already collapsed to ≈0.5 bits by the time it fires.

GSM8K (column 3) shows the opposite regime and illustrates the late-stabilization mechanism characterized in Section 4.1, the identical trajectory Prophet fails on in column 1: the answer position is still under a fully- or partially-masked span for most of the trajectory, so c_t is undefined there (dotted gray baseline, row 2); there is nothing to verify a candidate against yet, unlike Prophet's gap statistic, which stays defined (and noisy) even over pure mask tokens. Once the span is populated the candidate genuinely oscillates across 6 distinct values before settling on the correct one, 21; the gate withholds commitment until step 178 of 256 (70% of budget), since run$_t$'s required threshold has itself grown from the accumulated flip count (changes$_t$=17 by the time it fires); the same run-length that would have looked sufficient on a stability-only gate early in the trace is not sufficient here, because this trace has already shown itself to be unreliable. On this exact same model output, Prophet commits 39 steps earlier to a garbled non-answer; our gate waits and gets it right.

The literal decoded text, not just the signal traces above. Figure 8 shows the actual decoded buffer underlying the GSM8K trace just discussed (gt= 21) at each method's own commit point (step counts in each column header), not a stylized transcript. *Baseline* and *Prophet* share the exact same decode up to Prophet's trigger step; C^4 is the same trajectory replayed under our own gate. Baseline runs to completion and is correct; Prophet's one-shot fill lands on a truncated, garbled tail with no extractable number at all, while C^4 commits correctly with budget still unspent. We observed the same mechanism on MATH, including cases where the reasoning remained correct throughout but Prophet's one-shot fill corrupted only the final `\boxed{}` span itself, the one part of the derivation the whole answer depends on; Figures 9 and 10 repeat the same comparison on SVAMP and PIQA, showing the same one-shot-fill signature is not specific to this single GSM8K trajectory.

Prompt: Liam and Mitchell own competing lemonade stands across the street from one another. When Liam bragged that he had made $63 one weekend, Mitchell laughed and told Liam he had sold 21 lemonades at $4 apiece the same weekend. How many more dollars did Mitchell make selling lemonade that weekend than Liam?

Baseline (256/256 steps) ✓ Correct

To determine how many more dollars Mitchell made compared to Liam, we need to follow these steps:

1. Calculate Mitchell's earnings:

Mitchell sold 21 lemonades. Each lemonade was sold for $4. Therefore:

21 x 4 = 84 dollars

2. Determine the difference:

Liam made $63. Mitchell made $84.

84 - 63 = 21 dollars

So, Mitchell made $21 more than Liam.

Prophet (139/256 steps) ✗ Wrong

To determine how many more dollars Mitchell made compared to Liam, we need to follow these steps:

1. Calculate Mitchell's earnings:

Mitchell sold 21 lemonades. Each lemonade was sold for $4. Therefore:

21 x 4 = 84 dollars

2. Determine the difference:

Liam made $63. Mitchell made $84.

84 - 63 = 21 dollars

So, Mitchell made $21 more than than..

(one-shot fill froze mid-flicker; no number extractable)

C4 (178/256 steps) ✓ Correct

To determine how many more dollars Mitchell made compared to Liam, we need to follow these steps:

1. Calculate Mitchell's earnings:

Mitchell sold 21 lemonades. Each lemonade was sold for $4. Therefore:

21 x 4 = 84 dollars

2. Determine the difference:

Liam made $63. Mitchell made $84.

84 - 63 = 21 dollars

So, Mitchell made $21 more dollars than Liam.

(committed here; budget left unspent)

Figure 8: Literal decoded text at each method's own commit point. Qualitative comparison for one real GSM8K trajectory (gt= 21), the same trace as Figure 7. Extracted final answer highlighted in blue (correct); Prophet's one-shot fill leaves no number to extract at all.

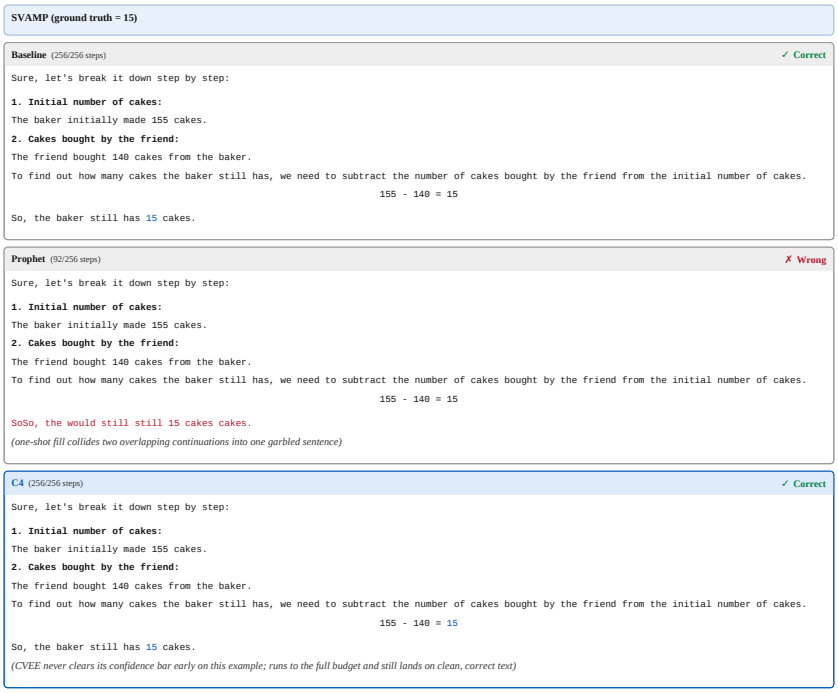

Figure 9: A third real trajectory (SVAMP). The same literal-decoded-text comparison as Figure 8. CVEE correctly declines to commit early when nothing in the trajectory clears its confidence bar, rather than forcing an early exit regardless.

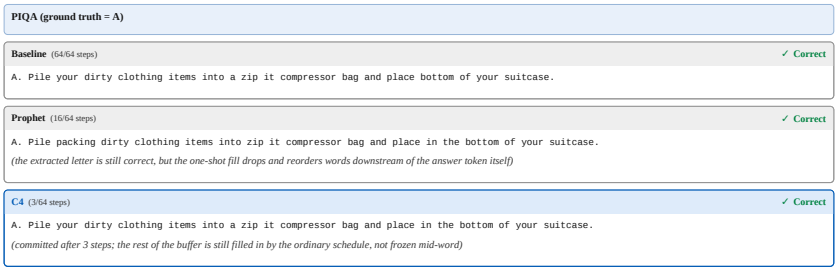

Figure 10: A fourth real trajectory (PIQA). The same literal-decoded-text comparison as Figure 8. Even where Prophet's *extracted* letter is still correct, its one-shot fill can leave the surrounding text measurably more garbled than either *Baseline* or C^4, a formatting cost the accuracy metric alone does not capture.

E Scaling and Composition

Scaling along each dimension. Table 7 separates generation length, block count, and block size. The strongest trend is with generation length: on GSM8K at fixed B=32, saving rises from 65.1% at L=128 to 84.0% at L=512. Prophet scales usefully on neither code nor GSM8K, where what rises is misfire rate rather than speed; only on MMLU does it scale safely, and there at a lower slope than C^4.

Composing with orthogonal accelerators. C^4 decides *how many* forward passes are taken, leaving the cost of one pass to other methods such as KV caching, suffix pruning (Chen et al., 2025), and step distillation (Deschenaux & Gulcehre, 2025; Zheng et al., 2026). Adding CVEE to WINO removes a further 70–76% of the steps it still spends on short-answer tasks at unchanged accuracy, while on GSM8K, SVAMP, and HumanEval no setting both fires and stays within tolerance; Appendix F gives the grid behind that second half. Stacking is not automatically free, though: the + DualCache column costs 7.3 points on HumanEval and 5.0 on SVAMP, gains 2.0 on GSM8K, and takes slightly *more* steps.

				C^4					+ DualCache					Fast-dLLM (DualCache+parallel)				
L	B	N	Baseline	Acc	Step	Saving	TPS	Speedup	Acc	Step	Saving	TPS	Speedup	Acc	Step	Saving	TPS	Speedup
HumanEval (code generation), block length swept at fixed generation length 384																		
384	16	24	41.5	39.6	44.5	88.4%	104.5	7.56×	32.3	45.4	88.2%	127.1	9.22×	39.0	64.4	83.2%	102.2	7.41×
384	32	12	40.2	42.1	39.4	89.7%	120.0	8.69×	34.8	44.7	88.4%	154.3	11.20×	37.8	57.2	85.1%	132.2	9.58×
384	64	6	39.6	42.1	36.5	90.5%	128.7	9.30×	36.6	42.2	89.0%	137.9	10.01×	36.6	51.1	86.7%	143.1	10.38×
GSM8K (long-reasoning), generation length swept at fixed block length 32																		
128	32	4	66.0	67.0	44.7	65.1%	77.3	2.51×	63.0	48.5	62.1%	51.7	1.70×	68.0	58.4	54.4%	45.0	1.48×
256	32	8	66.0	64.0	62.5	75.6%	67.5	3.55×	66.0	68.0	73.5%	75.1	3.97×	66.0	80.4	68.6%	63.6	3.36×
512	32	16	72.0	72.0	81.8	84.0%	75.8	5.84×	75.0	88.0	82.8%	108.2	8.34×	73.0	101.9	80.1%	92.4	7.13×
GSM8K (long-reasoning), L and B scaled together at fixed block count 8*, so r is held constant*																		
128	16	8	65.0	68.0	47.2	63.1%	73.2	2.39×	66.0	52.4	59.0%	54.5	1.79×	66.0	60.8	52.5%	44.8	1.47×
256	32	8	66.0	64.0	62.5	75.6%	67.5	3.55×	66.0	68.0	73.5%	75.1	3.97×	66.0	80.4	68.6%	63.6	3.36×
512	64	8	70.0	77.0	76.8	85.0%	77.2	5.94×	72.0	80.2	84.3%	115.4	8.90×	74.0	97.0	81.1%	99.8	7.69×
MMLU (short-answer), generation length swept at fixed block length 16																		
16	16	1	56.5	58.0	4.0	75.2%	128.3	3.83×	55.5	4.5	72.1%	82.9	2.80×	55.0	6.2	61.4%	59.3	1.96×
32	16	2	61.5	62.5	4.0	87.5%	247.2	7.37×	59.0	4.6	85.6%	147.9	4.94×	59.5	7.5	76.7%	93.3	3.12×
64	16	4	64.0	64.0	4.8	92.5%	490.4	16.16×	60.0	5.1	92.1%	355.5	12.07×	59.5	20.2	68.4%	77.8	2.66×

Table 7: Scaling along each dimension separately. Each panel moves one dimension and pins the others; the MMLU panel runs the other way from the rest, since CVEE stops those sequences before the last blocks are reached at all, so added blocks are never decoded rather than decoded cheaply. The backbone is LLaDA-8B-Instruct throughout.

F Composing CVEE with a Third-Party Sampler

The scaling appendix shows that C^4 composes with accelerators that reduce the cost of a forward pass rather than their number. The sharper question is whether its exit gate composes with a rival *sampler*, and WINO is the strongest one available to ask it of. Their loop runs until every position of every block is filled, so it makes no termination decision at any point, and CVEE makes only that decision from x_0 and the softmax probability of x_0, both of which their step already computes. The composition therefore costs no additional forward pass. CCTC is deliberately not composed, since it decides which positions a step may commit, which is the decision WINO's accept-and-revoke rule already makes.

The result splits by regime, and the split is the finding. Table 8 reports it. On the two short-answer tasks the deployed CVEE configuration removes a further 70–76% of the steps WINO still spends, at accuracy unchanged or half a point better. On long-reasoning and code the same configuration fires far too early and costs 23 to 36 points. That is not a tuning failure. We grid-searched the gate over $\tau_{\text{CVEE}} \in \{0.7, 0.8, 0.9\}$, $p_{\min} \in \{3, 5, 8, 12, 16\}$ and $\gamma \in \{2, 4, 8\}$, 45 settings per task, and the accuracy recovers monotonically as the bar rises only because the gate stops firing. At the setting that first comes within 2.0 points of WINO it fires on 14 of 100 GSM8K examples and saves 1.4% of the steps; there is no operating point on any of the three that both fires and holds accuracy.

Why it fails where it does. Two things are visible in the grid. WINO alone already spends 49.2 of 256 steps on GSM8K, and what remains is the segment in which the answer is still being decided, so there is no slack left for an exit gate to take; on MMLU it leaves 16.8 steps against an answer that settles by the fourth, and the slack is real. Separately, τ_{CVEE} is inert. All three values give identical accuracy at every $(p_{\min}, \gamma)$ on all three tasks, so the confidence condition never binds. WINO accepts

	WINO		+ CVEE, deployed		+ CVEE, best that holds	
Task	Acc	Step	Acc	Step	Acc	Step
Short-answer, where the answer settles inside the first block						
MMLU	61.0	16.8	61.5	4.1	–	–
HellaSwag	73.0	12.9	73.0	3.9	–	–
Long-reasoning and code, where WINO has already compressed the trajectory						
GSM8K	72.0	49.2	36.0	43.6	70.0	48.5
SVAMP	85.0	45.6	62.0	41.7	83.0	45.1
HumanEval	37.8	54.2	14.6	29.7	36.6	50.1

Table 8: CVEE composed onto WINO's sampler, LLaDA-8B-Instruct. Deployed is the frozen configuration used everywhere else in this paper, never re-tuned for the composition. "Best that holds" is the grid setting with the fewest steps whose accuracy stays within 2.0 points of WINO, and it is reported only where the deployed configuration fails; it fires on 14/100, 17/100 and 47/164 examples respectively, which is why it saves so little. Same n and evaluation examples as Table 1.

positions inside the answer span at a threshold of 0.5, and the high confidence CVEE then measures there is the sampler's own commit rather than convergence. That is the contamination of Section 1 measured on a sampler we did not design, and it is the reason CCTC commits the answer span only as part of a boundary-anchored core that a confirmation round has survived, rather than letting any single confident token pin it.

G Sensitivity

G.1 Speedup Decomposition and Peer Settings

Two peer settings used in Table 7 are worth stating here rather than in its caption. Fast-dLLM runs from its own released implementation at its published threshold 0.9 with its KV cache disabled, so that every step count in that table means uncached model calls; enabling the cache would raise its wall-clock speedup above the step ratio shown. Its Dream cells are left unmeasured because that acceleration ships only on a cached block path, which we would have to modify to keep the column's cost model uniform.

G.2 Gap-Budget Sensitivity

The gap budget H controls how many unresolved low-confidence holes CCTC's boundary-anchored core may cross. At H=0 the core is strictly contiguous; H=∞ removes the hole limit and, consequently, the structural deferral path. We vary $H \in \{0, 1, 2, 4, \infty\}$ on one representative task from each regime while holding every other C^4 setting fixed. This is a sensitivity rerun, not a second estimate of Table 1: accuracy and TPS are therefore reported relative to the H=1 cell within the same sweep, and no absolute main-table cell is replaced.

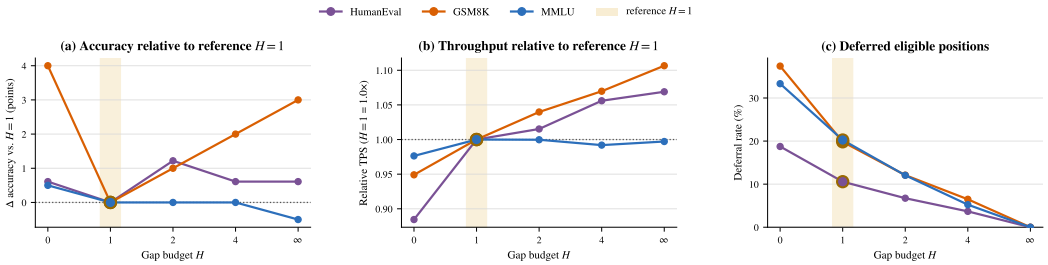

Figure 11: Gap-budget sensitivity on LLaDA-8B-Instruct. Accuracy and throughput are normalized to the reference H=1 cell within the sweep. Increasing H monotonically reduces structural deferral and generally raises throughput, while accuracy shows no monotone degradation. The shaded H=1 column marks the fixed reference, not a per-task optimum; H=∞ is the mechanism endpoint with no structural deferral rather than a recommended deployment setting.

Moving from strict contiguity (H=0) to H=1 raises TPS by 13.1%, 5.4%, and 2.4% on HumanEval, GSM8K, and MMLU, respectively, while reducing the corresponding deferral rates from

18.7/37.4/33.3% to 10.6/19.8/20.2%. Across the full sweep, accuracy differs from the within-sweep H=1 reference by at most 1.2, 4.0, and 0.5 points on the three tasks. We make no claim that H=1 maximizes either accuracy or throughput: it is a conservative, globally fixed setting that relaxes the strict H=0 core while keeping deferred confirmation active.

G.3 Per-Block and Total-Step Behavior, All Tasks

The same measurements, extended to all 12 tasks, both models. Figure 6 in the main text shows a 3-task/LLaDA-only subset; Figures 12–17 repeat the identical protocol across the full 12-task, 2-model matrix, confirming the same pattern throughout: short-answer tasks finish within one or two blocks while long-reasoning ones spend most of their budget late, the dichotomy Section 4.1 characterizes.

The same per-block usage, totaled into one bar per method. Figures 14 and 15 lay the same per-block segments end to end into a single bar per method, with accuracy shown as a thinner bar beneath so step savings can be compared against whether they cost accuracy. At the deployed setting, C^4's accuracy bar stays within tolerance of *Baseline*'s on every short-answer task regardless of step-bar length, though peer methods can deviate more, while on long-reasoning tasks Prophet's and SlowFast's accuracy bars shrink visibly even where their step bars match C^4's, the same severe-drop pattern Table 1 reports as numbers.

Per-block wall-clock share: which block is actually the bottleneck. Figures 16 and 17 break the same data down by *time* instead of step count; segment width is that block's estimated share of wall-clock time under the uniform-per-step apportionment, while the right-hand label is the directly measured aggregate RTX 4090 TPS from Table 1. It is not an independent per-block timing, and TBD marks a sensitivity setting not timed on this card. The breakdown makes "final filling" legible; on long-reasoning tasks, the final block's time share grows toward the full bar under C^4 simply because every other block has been cut so much its fixed cost now dominates.

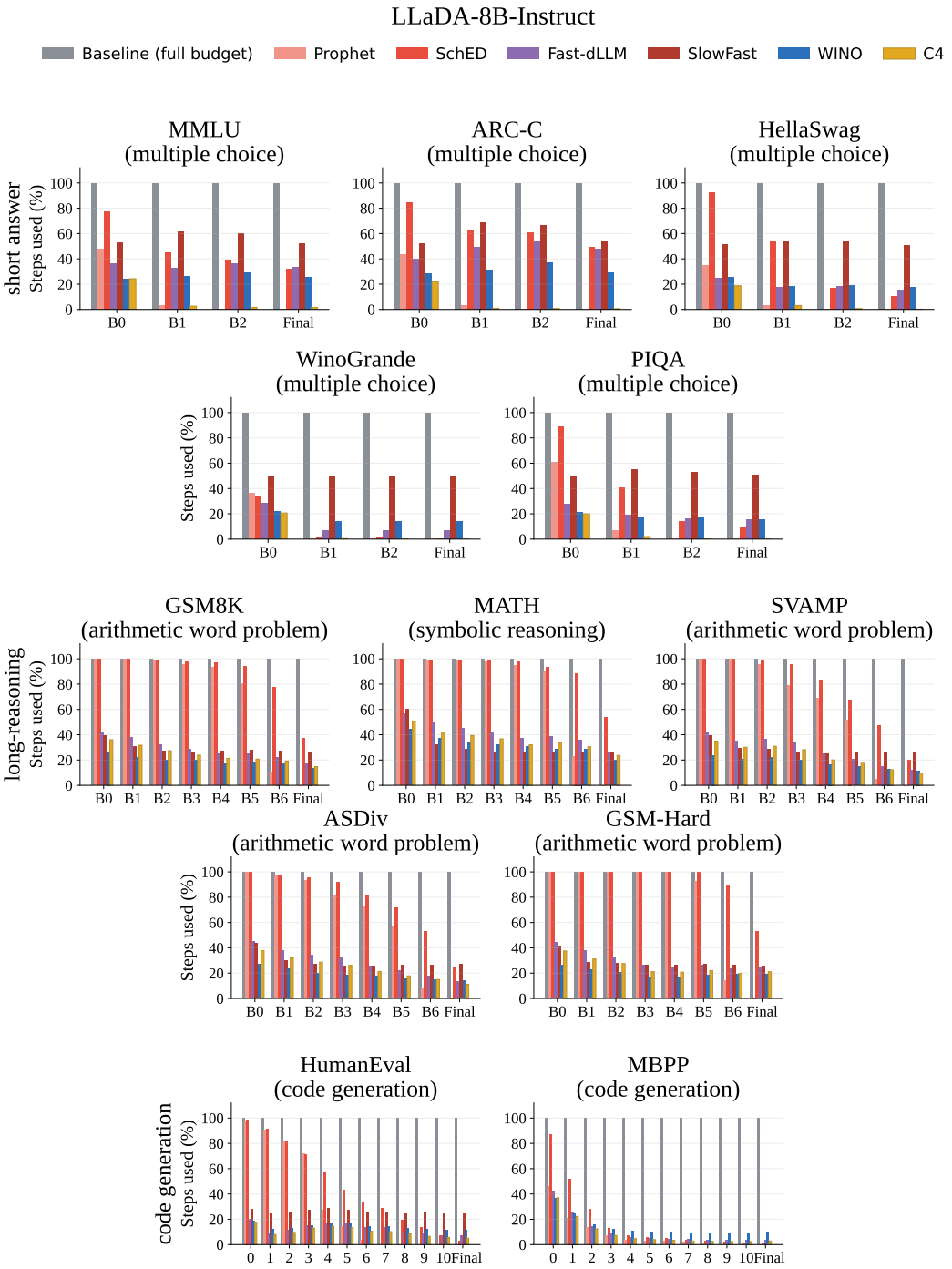

Figure 12: Per-block step usage, all 12 tasks, LLaDA-8B-Instruct. One row per regime; each panel names the task and what kind of task it is.

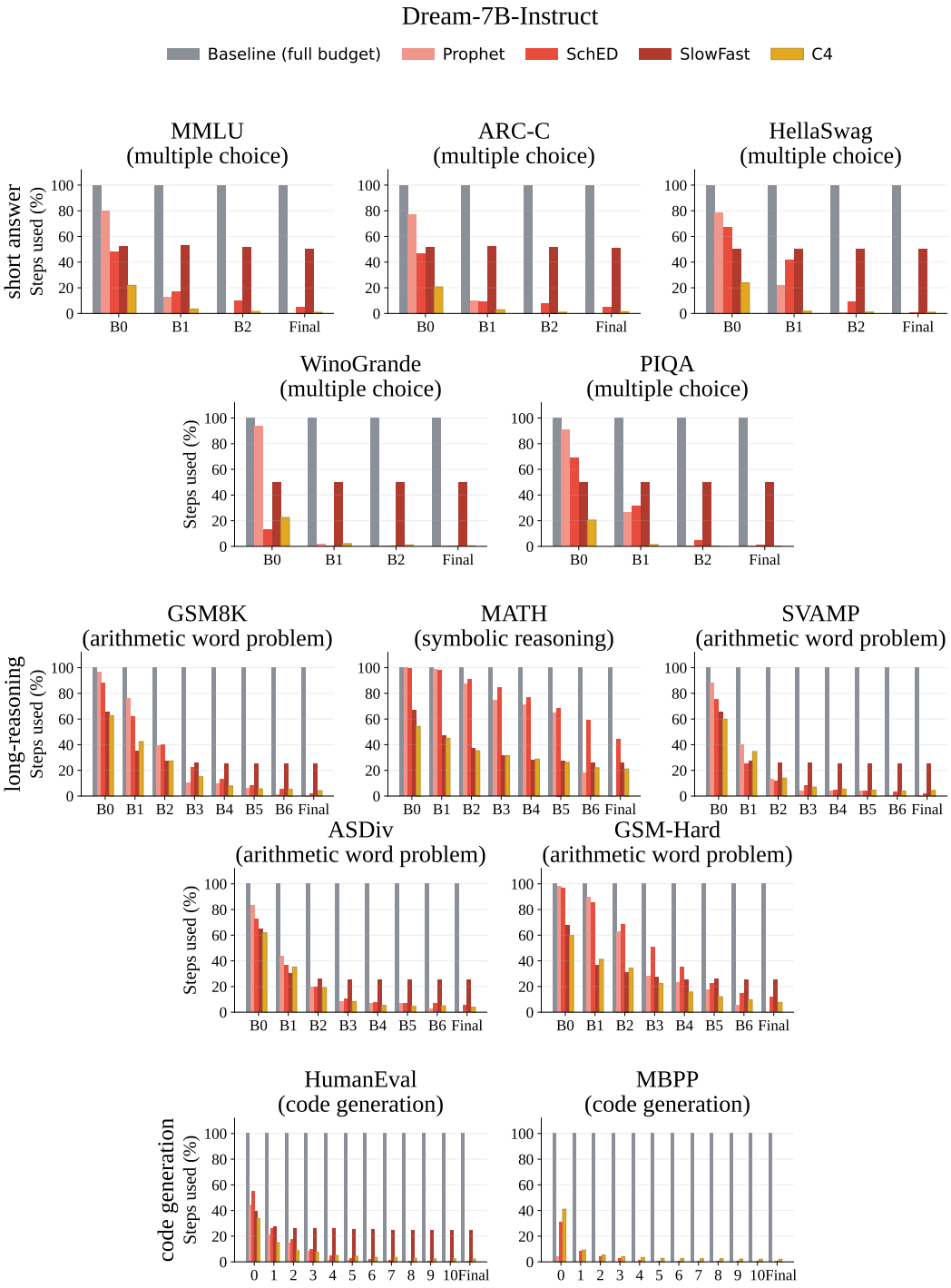

Figure 13: Per-block step usage, all 12 **tasks, Dream-7B-Instruct.** Same protocol and layout as Figure 12.

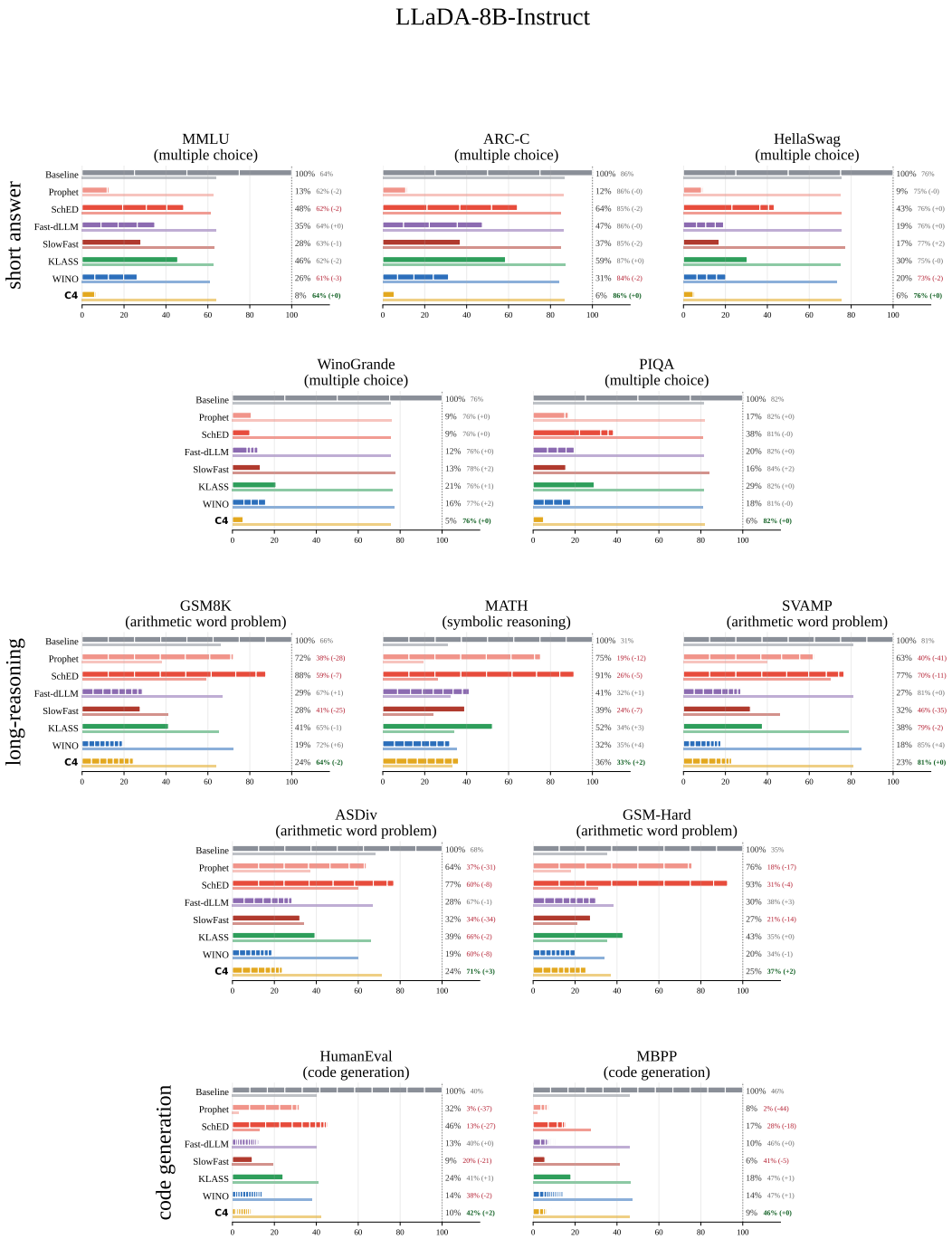

Figure 14: Total steps and accuracy, all 12 tasks, LLaDA-8B-Instruct. Thick bars are total steps used, thin bars beneath are accuracy.

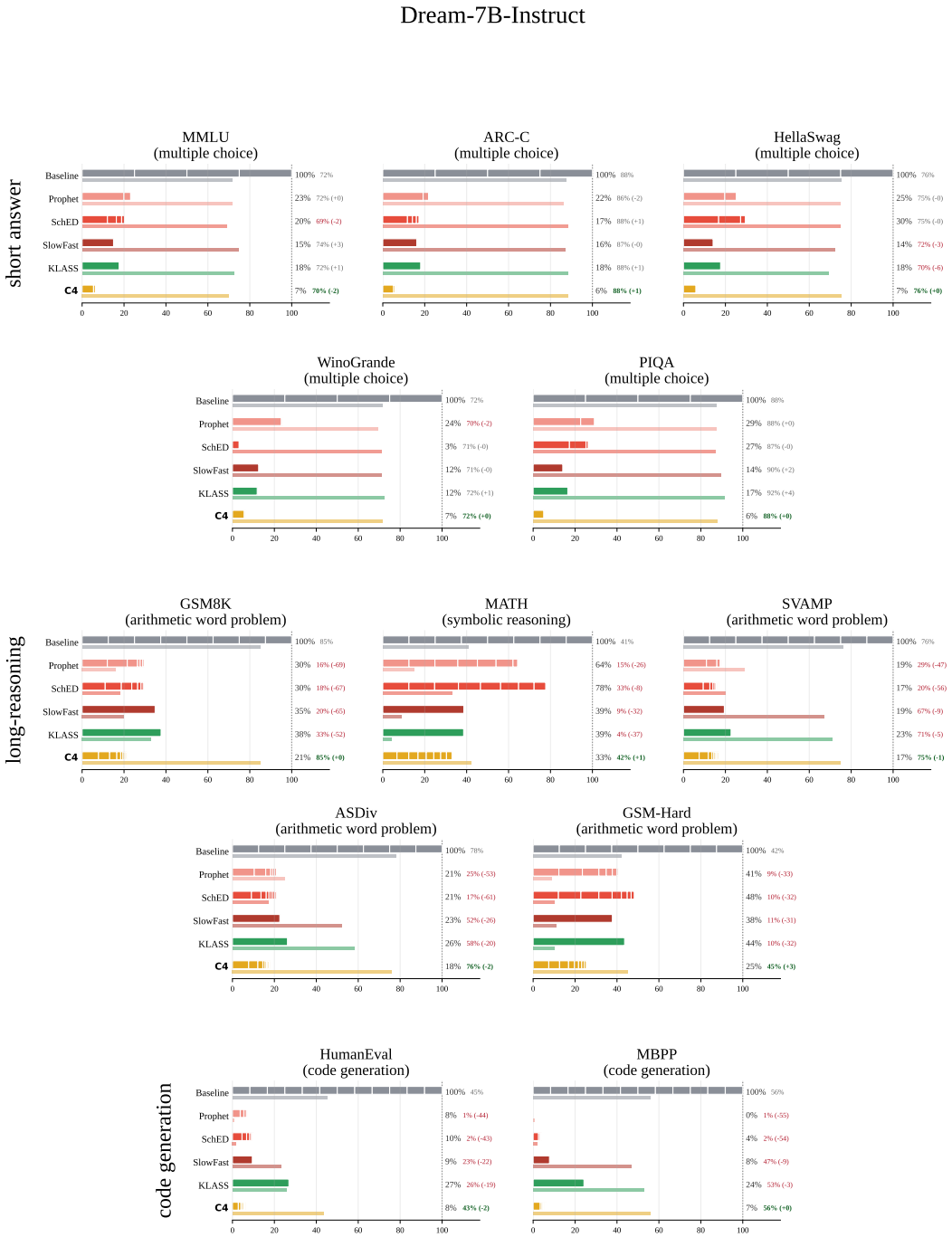

Figure 15: Total steps and accuracy, all 12 tasks, Dream-7B-Instruct. Same protocol and layout as Figure 14.

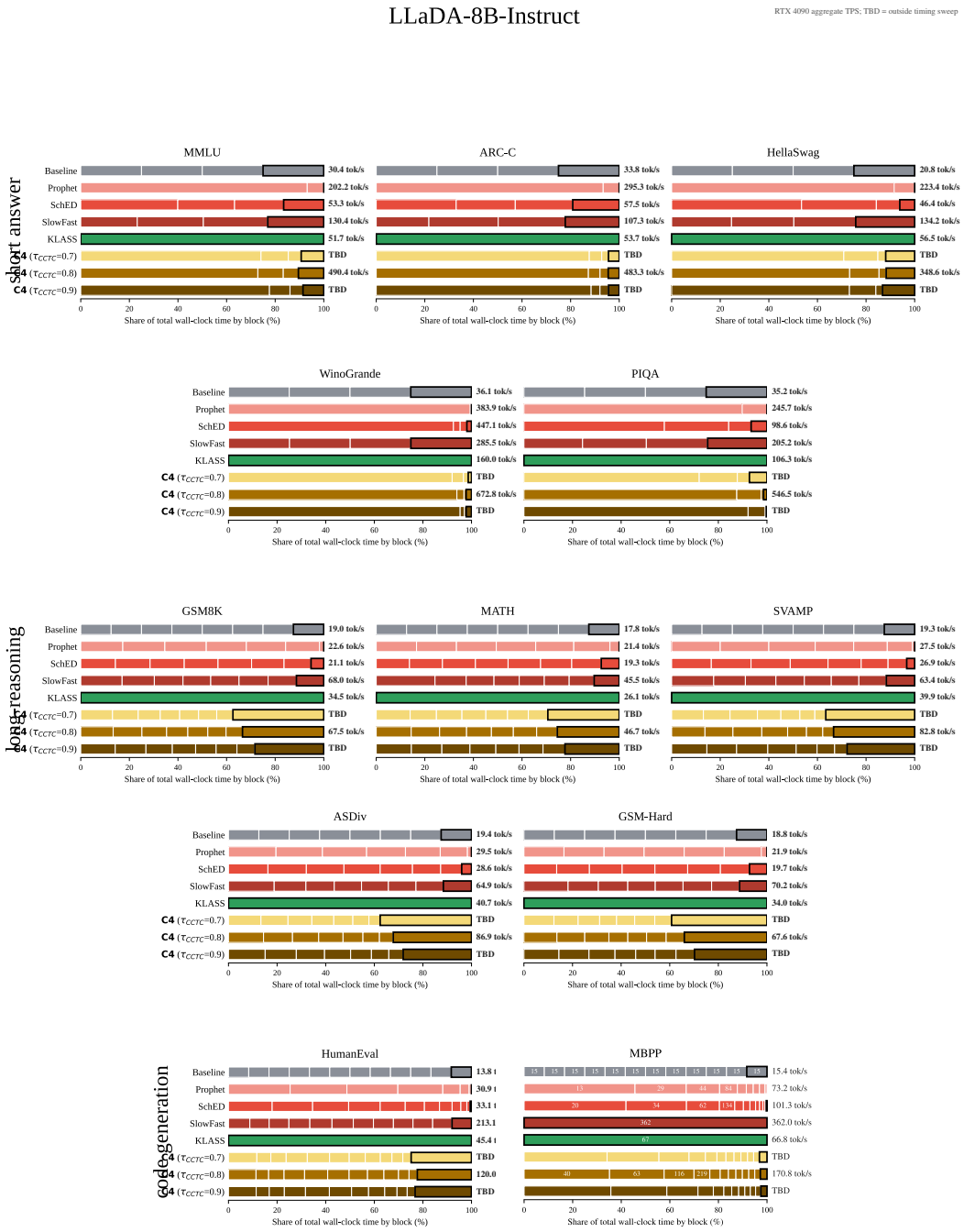

Figure 16: Per-block wall-clock share, all 12 tasks, LLaDA-8B-Instruct. Step-share-based wall-clock apportionment with verified aggregate RTX 4090 TPS at right. The deployed setting is τ_{CCTC}=0.8; sensitivity-only rows outside the formal timing sweep remain TBD. For MBPP, aggregate-only peer rows are left undivided rather than assigned a fabricated block split.

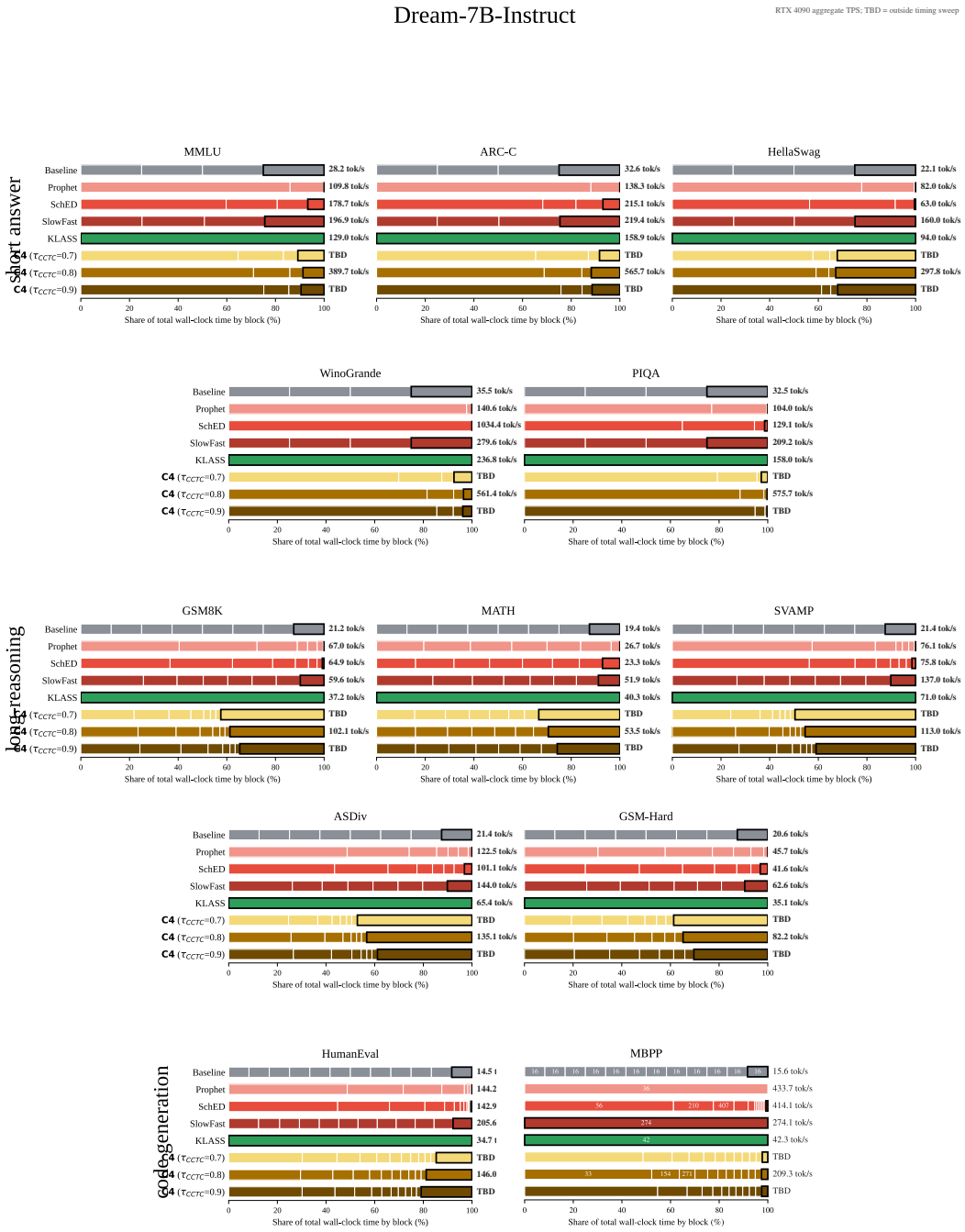

Figure 17: Per-block wall-clock share, all 12 **tasks, Dream-7B-Instruct.** Same protocol and TBD policy as Figure 16.

H Limitations

- **Requires a delimitable answer unit.** CVEE needs an answer unit that the task's own output format delimits, so that a deterministic parser can pull it out of the buffer and relocate it at every step. Fixing where that parser looks and what it looks for is a structural prior CVEE's design requires rather than a hyperparameter tuned per task, as Appendix A.2 sets out. The unit itself need not be short. It is a single letter on the six short-answer tasks and a number or a boxed expression on the five long-reasoning ones, while on HumanEval it is the generated function in its entirety, delimited by Python's own indentation structure, and the gate governs termination there under the same frozen tuple of Table 1. What the requirement genuinely excludes is output that delimits no unit at all. Open-ended prose is the clearest such case, since a free-form summary offers no sub-span an extractor could track and relocate. CCTC alone still applies to non-final blocks of a multi-block generation there, while the answer-verification half of the gate has no defined target, so C^4's termination guarantee does not extend to such tasks.

- **Evaluated under greedy decoding.** Every number in this paper is produced at temperature 0, the protocol the compared accelerators and the pass@1 and exact-match benchmarks themselves use, so we have not measured C^4 where a single prompt is expected to yield diverse samples. The two gates would not be affected equally. CCTC thresholds a genuine softmax probability and constrains the arrangement of the committed positions, neither of which refers to how the committed token was chosen, so the rule carries over unchanged. CVEE is the part that assumes a deterministic realization, since its stability term counts consecutive steps on which the extracted candidate is unchanged, and under sampling that string fluctuates even once the underlying distribution has settled. The consequence follows from the form of Eq. 4 rather than from measurement, and it is conservative. A resetting run counter and a growing change count both raise the bar $\max(p_{\min}, \lceil \gamma\, \text{changes}_t \rceil)$, so the gate fires later or not at all, giving up speedup rather than committing early. The natural adaptation is to decouple the signal the gate verifies from the token the decoder emits, tracking stability on the top-1 of the noise-free distribution over the answer span while sampling proceeds normally. Both quantities are already computed at every step, so this costs no additional forward pass, but it changes what is certified from the identity of one realized string to the convergence of the model's belief about the answer. Whether that weaker certificate preserves the accuracy bound is an open question we do not settle here.

- **Commits are monotonic.** All of C^4's commits are also monotonic; once a position clears CCTC's threshold or scheduled top-k quota, it is never revisited, even if a later step's now-richer context would predict it differently. CVEE's joint gate protects only the final answer span this way; an intermediate reasoning token committed under CCTC's cheaper, non-final-block rule has no equivalent safety net. A mask-and-reconstruct verification pass, checking whether the model's own updated context would reconstruct the same candidate before committing, could provide an additional safety check, but would require an extra forward pass per candidate, directly competing with the speedup this paper targets; evaluating this trade-off, and whether the cost is better reinvested to justify a lower, more aggressive τ_{CCTC}, is left to future work.

- **Extending beyond a single tracked unit.** CVEE's verification targets one identity-tracked unit per example, which on HumanEval is the single function each prompt asks for. Outputs assembled from several independent units fall outside that design, a multi-function program or a multi-hop response being the natural cases, and falling back to whole-buffer distributional stability would collapse into the same aggregate-confidence failure mode Section 4.1 identifies in Prophet, not a genuine extension of CVEE's own logic. A more promising route decomposes the output into candidate units and applies CVEE's identity-and-stability test per unit; CCTC's final-block asymmetry would also need a different structural prior once no block is privileged this way. Pursuing this decomposition, and adding distribution-free risk control (Xie et al., 2026; Wynn et al., 2026) on top of the empirical tolerance used throughout this paper, are natural next steps.